

Generation of squeezed states of light with a fiber-optic ring interferometer

R. M. Shelby, M. D. Levenson, D. F. Walls,* and A. Aspect†
IBM Almaden Research Center, 650 Harry Road, San Jose, California 95120-6099

G. J. Milburn

Australian National University, Canberra, P.O. Box 4, Australian Capital Territory, Australia 2600

(Received 19 November 1985)

Forward nondegenerate four-wave mixing in an optical-fiber ring resonator is proposed as a method to generate squeezed states of light. The nonlinear interactions are analyzed both with a self-consistent propagation-equation technique and with Fokker-Planck equations in the Glauber-Sudarshan P representation. Excellent squeezing is predicted at modest input power levels, with perfect quantum-noise squeezing at the critical points for optical bistability. A method to suppress the stimulated Brillouin effect is proposed and demonstrated experimentally, and the effects of forward spontaneous guided acoustic wave Brillouin scattering inside the resonator are analyzed. Methods are suggested for minimizing this noise under conditions where squeezing can be detected. Experimental apparatus and procedures are outlined for verifying the predictions of our theory and demonstrating squeezing of classical and quantum noise.

I. INTRODUCTION

Squeezed states of light are quantum states in which the fluctuations in one phase quadrature amplitude are less than those for a coherent state.¹ Such states have been predicted theoretically, and various experimental methods are being pursued in attempts to demonstrate their existence.²⁻⁴ The underlying experimental difficulty is that the nonlinear optical interactions that create squeezing are very weak while undesirable effects—such as attenuation and diffraction—can be quite strong. We have previously proposed nondegenerate four-wave mixing in an optical fiber as a means of circumventing these difficulties.⁴ A different strategy, making use of a “one-port optical cavity” to enhance the squeezing interactions has also been proposed.⁵⁻⁹ The purpose of this paper is to describe how the two techniques can be profitably combined in a fiber-optic ring interferometer and to present some preliminary experimental results.

The overall scheme of squeezed-state generation by forward nondegenerate four-wave mixing in an optical fiber has been thoroughly reviewed in two previous papers.^{4,10} Basically, a strong single-frequency pump wave at frequency ω_p interacts with two weak fluctuating sideband amplitudes at ω_s and ω_l which fulfill $\omega_s - \omega_p = \omega_p - \omega_l = \Omega_N$. The sideband fluctuations become correlated by the nonlinear process, and a shift in the phase of the pump wave with respect to the sidebands can reveal squeezing. Nonlinear dispersion shifts the phase of the squeezed quadrature as the squeezing effect increases.¹⁰

The nonlinear interaction that mixes the pump and sidebands to cause squeezing of the sidebands also alters the phase of the pump light. In a fiber cavity, the result is optical bistability, with consequent enhancement of the squeezing effects as predicted for the degenerate case.⁹ All of these issues will be treated in the second section of this paper which describes the nonlinear interactions in depth.

The recent developments of low-loss fibers and variable couplers have made fiber nonlinear optics experiments such as this feasible. However, two serious experimental difficulties must be overcome before squeezed states can be generated in a ring cavity. First, parasitic effects—principally stimulated Brillouin scattering (SBS)—must be suppressed.¹¹ The technology developed to eliminate SBS in the traveling-wave case is not entirely appropriate to a ring resonator. Another technique employing a fiber-optic “diode” inside the ring resonator will be described in Sec. III. Also the excess phase noise caused by forward guided-acoustic-wave Brillouin scattering (GAWBS) must be dealt with somehow.¹² In the output of a fiber ring interferometer, GAWBS need not be pure phase noise, and strategies to minimize it in the squeezed quadrature of the output wave will be described in Sec. IV.

Section V describes our proposed experiment and the results predicted by this theoretical treatment. Near the critical points for optical bistability, we predict very large squeezing of the sidebands at frequencies shifted from the pump by multiples of the free spectral range of the ring cavity. The parameters of the proposed experiment seem sufficiently feasible to motivate an aggressive experimental program.

II. SQUEEZING AND OTHER NONLINEAR EFFECTS IN A FIBER-OPTIC RING INTERFEROMETER

A. Fiber ring resonator

A fiber-optic ring resonator basically consists of a loop of single-mode optical fiber in which a fraction of the output is coherently coupled back into the input by an evanescent-wave directional coupler as shown in Fig. 1.¹³ Short lengths of fiber on each of the other ports of the coupler serve for input and output. Such ring interferom-

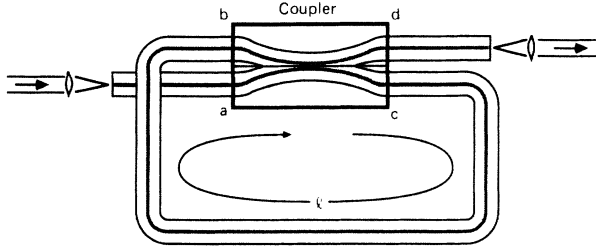


FIG. 1. Schematic of a fiber ring interferometer. The light from the laser is coupled into the core of the fiber where it propagates as a single guided mode. The fibers within the directional coupler are polished flat on one side so that the evanescent fields leaking from the core overlap. The labeling of the ports of the coupler in this figure is used throughout the paper. The length of the light path around the resonator is l .

eters have been used as low-threshold-stimulated Brillouin ring lasers and have been proposed for other applications.^{14,15} In our experiments, the stimulated Brillouin effect and other parasitic phenomena must be suppressed by additional elements within the ring, but the basic design shown in Fig. 1 serves to explain the physics of the nonlinear interactions.

Optical power is coupled from the input port a of the directional coupler to the output port d with efficiency η and also from port b to c with efficiency η . The net phase shift for transmission from port a to d and from port b to c is ϕ_c . (For purposes of exposition $\phi_c = \pi$.) Typically η can be varied between 0 and 0.98, and plays the role of the reflectivity of the input mirror in a conventional ring interferometer. The coupler itself and the loop of fiber attenuate the circulating optical powers by scattering and absorption. The per pass loss (excluding the coupling η) is $L = 1 - \gamma$. The length of the optical path around the resonator is l and the free spectral range is thus

$$\Omega_c = 2\pi c / nl,$$

where n is the effective index of refraction of the fiber. When the input and circulating optical powers are sufficiently low such that all nonlinear effects can be ignored, the circulating and output optical amplitudes at the frequency ω are

$$E^c = E^b e^{-i\Phi} = \frac{\sqrt{\gamma(1-\eta)}}{1 - \sqrt{\gamma\eta} e^{i\Phi}} E^a \quad (1)$$

and

$$E^d = -\sqrt{\gamma\eta} \left[1 - \frac{\sqrt{\gamma/\eta}(1-\eta)e^{i\Phi}}{1 - \sqrt{\gamma\eta}e^{i\Phi}} \right] E^a, \quad (2)$$

where $\Phi = nl\omega/c$ is the phase delay for a round trip through the fiber loop for a wave of frequency ω .¹⁶ For the case of interest here $(1-\gamma) \ll (1-\eta)$, it is convenient to simplify the above equations by omitting all but the nearest cavity resonance for each of the three frequencies of interest. Introducing a detuning for the wave E_i at frequency ω_i from the nearest cavity resonance Ω_i ,

$$\Delta_i = \omega_i - \Omega_i = \left[\frac{\Phi}{2\pi} - m \right] \Omega_c,$$

and writing $\gamma = 1 - \epsilon 2\pi / \Omega_c$ and $\eta = 1 - \xi 2\pi / \Omega_c$ where we assume $\epsilon, \xi \ll \Omega_c / 2\pi$ we obtain the following approximations to the cavity resonance:

$$E_i^c = \frac{\left[\frac{\sqrt{\xi\Omega_c/2\pi}}{\left[\frac{\epsilon + \xi}{2} \right] - i\Delta_i} \right] E_i^a, \quad (3)$$

$$E_i^d = \frac{\left[\Delta_i^2 + \left[\frac{\epsilon^2 - \xi^2}{2} \right] - i\xi\Delta_i \right]}{\Delta_i^2 + \left[\frac{\epsilon + \xi}{2} \right]^2} E_i^a, \quad (4)$$

$\kappa = (\epsilon + \xi)/2$ is the cavity linewidth [half width at half maximum (HWHM)] due to damping of radiation inside, $\Omega_i = \Omega_{i-1} + \Omega_c$ and Ω_c is the free spectral range of the resonator. This treatment approximates the Airy function linewidth in the limit $\eta \rightarrow 1$. In the Appendix we give an alternative derivation of the main theoretical results which avoids this approximation by obtaining a simultaneous self-consistent solution for the steady-state pump wave and a single pair of sidebands.

B. Nonlinear interaction and bistability

The nonlinear optical susceptibility of the fused silica fiber causes the phase shift between ports c and b to vary with the circulating power. This leads to dispersive optical bistability. We will assume that only the nonresonant optical nonlinearity is effective, and that it can be characterized by a single tensor element independent of frequency arguments:¹⁷

$$\begin{aligned} \chi_{1111}^{(3)}(-\omega_s, \omega_p, \omega_p, -\omega_l) &= \chi_{1111}^{(3)}(-\omega_p, \omega_p - \omega_p, \omega_p) \\ &= \chi^{(3)} = 5 \times 10^{-15} \text{ cm}^3/\text{erg}. \end{aligned} \quad (5)$$

In our time-domain treatment, an effective nonlinear coupling parameter $\chi \tilde{I}_c$ is defined by

$$\chi \tilde{I}_c = \frac{3\omega_p}{n^2} f \chi^{(3)} |E_p^c|^2 \quad (6)$$

where f is a mode overlap factor in the fiber which is approximately equal to 1.¹⁸ The tilde over $\tilde{I}_c, \tilde{E}_p^c$, etc., indicates that these are dimensionless quantities with magnitudes related to the number of photons. The squeeze parameters analogous to those in Ref. 10 will also be expressed as

$$r_j = \frac{12\pi\omega}{nc} f \chi^{(3)} |E_p^j|^2 l = \frac{4\pi\chi \tilde{I}_j}{\Omega_c}. \quad (7)$$

The input wave at the port a is assumed to consist of a strong pump wave at frequency ω_p which can be treated classically and very weak fluctuating fields at other frequencies which will be treated quantum mechanically. The steady-state equation for the mean circulating amplitude at frequency ω_p can be calculated using the classical

model of dispersive bistability:¹⁹

$$(\kappa - i\Delta_p)\tilde{E}_p^c - 2i\chi\tilde{I}_c\tilde{E}_p^c = \sqrt{\xi\Omega_c/2\pi}\tilde{E}_p^a, \quad (8)$$

where Δ_p is the detuning of the pump frequency from the center of a nearby cavity resonance and $\tilde{I}_c = |\tilde{E}_p^c|^2$. For bistable operation, we require $\Delta_p\chi < 0$. The familiar bistable state equation for the squares of the input and circulating amplitudes becomes

$$\frac{\xi\Omega_c}{2\pi} |\tilde{E}_p^a|^2 = \tilde{I}_c [\kappa^2 + (\Delta_p + 2\chi\tilde{I}_c)^2]. \quad (9)$$

The output wave is then

$$\tilde{E}_p^d = \sqrt{2\pi/\xi\Omega_c} \left[\left(\frac{\epsilon - \xi}{2} \right) - i(\Delta_p + 2\chi\tilde{I}_c) \right] \tilde{E}_p^c, \quad (10)$$

and the input, output, and circulating amplitudes are given in cgs units as

$$E_p^j = \sqrt{4\pi\hbar\omega/n^2V_Q}\tilde{E}_p^j,$$

where V_Q is the quantization volume of the fiber ring and the tilde indicates a dimensionless quantity given by the square root of the photon number.

C. Nondegenerate four-wave mixing

Pairs of frequencies are coupled together by the circulating pump mode via the nondegenerate four-wave mixing interaction familiar from coherent anti-Stokes Raman spectroscopy (CARS).¹⁷ Those frequencies are related by $\omega_s + \omega_I = 2\omega_p$ and the electromagnetic waves at these frequencies must be treated quantum mechanically. Outside the cavity, an infinite continuous set of pairs of such sideband modes exist with frequencies summing to $2\omega_p$. Since the nonlinear interaction takes place inside a cavity, our method will be to quantize the energies of the sidebands in units of the nearest cavity-mode frequencies. For the external wave at ω_s , that frequency is $\Omega_{p+m} = \Omega_p + m\Omega_c$ while for the external wave at ω_I , the mode frequency is $\Omega_{p-m} = \Omega_p - m\Omega_c$. These cavity modes will then be projected onto the free-space modes once their properties have been determined. In this Heisenberg representation, the operators a_+ and a_- os-

cillate at frequencies Ω_{p+m} and Ω_{p-m} , respectively. Including the largest energy conserving nonlinear terms, the Hamiltonian for the weak fields inside the cavity is

$$\begin{aligned} \mathcal{H} = & \hbar[(\Omega_p + m\Omega_c)a_+^\dagger a_+ + (\Omega_p - m\Omega_c)a_-^\dagger a_-] \\ & + \hbar\chi[4|\tilde{E}_p^c|^2(a_+^\dagger a_+ + a_-^\dagger a_-) \\ & + 2(\tilde{E}_p^c)^2 a_+^\dagger a_-^\dagger + 2(\tilde{E}_p^{c*})^2 a_+ a_-] \\ & + a_+ \Gamma_c^\dagger + a_- \Gamma_c^\dagger + a_+^\dagger \Gamma_c + a_-^\dagger \Gamma_c. \end{aligned} \quad (11)$$

The heat-bath operators representing the damping of the fields within the cavity are Γ_c . The relationships of the various frequency parameters are illustrated in Fig. 2. The pump-laser frequency is equal to the local oscillator frequency and denoted ω_p with the extra-cavity signal and idler sidebands ω_s and ω_I , respectively, spaced equally to either side by a shift Ω_N . The frequency dependence of the circulating power in the fiber ring is depicted as a solid curve, with dashed portions denoting regions where the approximations used are invalid. The detuning of the pump frequency from the cavity resonance just above it is $\Delta_p = \omega_p - \Omega_p$. In discussions of bistability the frequency of the “empty” cavity mode nearest the pump and fulfilling $\Delta_p\chi < 0$ is Ω_p . The spacing of the peaks of the figure is a multiple of the free spectral range Ω_c . The widths of the cavity resonances reflects the cavity damping rate κ . The frequency of the fluctuations detected electrically is Ω_N . A useful auxiliary quantity is the difference between Ω_N and m times the cavity free spectral range:

$$\Omega = \Omega_N - m\Omega_c.$$

It is useful to transform to an interaction picture given by

$$U(t) = \exp\{-i[(\omega_p + m\Omega_c)a_+^\dagger a_+ + (\omega_p - m\Omega_c)a_-^\dagger a_-]t\}. \quad (12)$$

Then using standard techniques we may derive stochastic differential equations for the c -number amplitudes α_+ and α_- associated with the operators a_+ and a_- .²⁰ The amplitudes α_\pm are equivalent to the quantities we have defined as \tilde{E}_i^c and are in units of the square root of photon number. The physical field amplitudes at frequencies

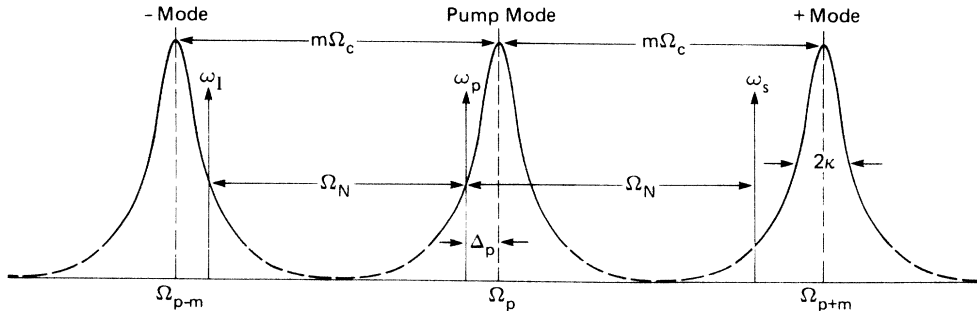


FIG. 2. Relationships of the interferometer mode, pump and noise frequencies. The free spectral range of the ring cavity is Ω_c . The modes of interest are spaced by $m\Omega_c$. The pump laser frequency is labeled ω_p and lies near the mode with frequency Ω_p . The detuning of the pump from that mode frequency is Δ_p , with $\Delta_p < 0$ for $\omega_p < \Omega_p$. The signal and idler frequencies are labeled ω_s and ω_I , respectively, and are shifted from the pump by $\pm\Omega_N$. The pair of modes nearest the signal and idler have frequencies Ω_{p+m} and Ω_{p-m} , respectively. The half width at half maximum of all the modes is κ . The frequency $\Omega = \Omega_N - m\Omega_c$.

$\omega_+ = \Omega_p + m\Omega_c$ and $\omega_- = \Omega_p - m\Omega_c$ are then given in cgs units by

$$E_{\pm}^c = \sqrt{4\pi\hbar\omega/n^2 V_Q} \alpha_{\pm}, \quad (13)$$

where $V_Q = Al$ is the quantization volume. The time and spatial dependence of the electric field in the cavity is given by

$$E_{\pm}(r,t) = 1/2 E_{\pm}^c F(x,y) \exp(-i\omega_{\pm}t - k_{\pm}z) + \text{c.c.}$$

and the transverse spatial profiles $F(x,y)$ are related to the effective mode area A by

$$A = \int |F(x,y)|^2 dx dy / |F(0,0)|^2$$

(see Ref. 4). The mean squares of these stochastic field amplitudes are nonzero. The equations of motion for the amplitudes α_+ and α_- of the cavity modes can then be derived from the Hamiltonian via a master equation and a Fokker-Planck equation in the Glauber-Sudarshan P rep-

resentation. These equations assume the form of stochastic differential equations where the fluctuating forces represent the quantum noise. Defining the fluctuation vector

$$\alpha = \begin{pmatrix} \alpha_+ \\ \alpha_+^* \\ \alpha_- \\ \alpha_-^* \end{pmatrix}. \quad (14)$$

The stochastic equation becomes

$$\frac{\partial \alpha}{\partial t} = \underline{A} \alpha + \underline{D}^{1/2} \Gamma(t), \quad (15)$$

where $\langle \Gamma_i(t) \Gamma_j(t') \rangle = \delta_{ij} \delta(t-t')$.

The drift and diffusion matrices may be derived using standard techniques,

$$\underline{A} = \begin{pmatrix} \kappa + i\Delta_p + 4i\chi\tilde{I}_c & 0 & 0 & 2i\chi\tilde{I}_c \\ 0 & \kappa - i\Delta_p - 4i\chi\tilde{I}_c & -2i\chi\tilde{I}_c & 0 \\ 0 & 2i\chi\tilde{I}_c & \kappa + i\Delta_p + 4i\chi\tilde{I}_c & 0 \\ -2i\chi\tilde{I}_c & 0 & 0 & \kappa - i\Delta_p - 4i\chi\tilde{I}_c \end{pmatrix}, \quad (16)$$

$$\underline{D} = \begin{pmatrix} 0 & 0 & -2i\chi\tilde{I}_c & 0 \\ 0 & 0 & 0 & 2i\chi\tilde{I}_c \\ -2i\chi\tilde{I}_c & 0 & 0 & 0 \\ 0 & 2i\chi\tilde{I}_c & 0 & 0 \end{pmatrix}. \quad (17)$$

and we have assumed the reservoir to be at zero temperature. The phase of the circulating field \tilde{E}_p^c in the cavity has been set to zero and $\tilde{I}_c = |\tilde{E}_p^c|^2$. This implies that the phase of the input wave E_p^a is nonzero and must be calculated from Eq. (8). The diffusion matrix is nonpositive definite in this four-dimensional formalism, allowing squeezing to be possible, but a positive definite D matrix can be defined using the positive P representation with an eight-dimensional fluctuation vector.²¹ Except for the delta-correlated fluctuating force $\Gamma(t)$ these equations are equivalent to those in Ref. 10 and include the effect of "nonlinear dispersion," which allows the pump wave to shift the phase of the signal and idler sidebands. In the case of a single mode, the normally ordered spectral matrix is defined as the Fourier transform of the time-ordered and normally-ordered correlation matrix⁹

$$\underline{S}(\Omega) = \int e^{i\Omega\tau} T : \begin{pmatrix} \langle a(t)a(t+\tau) \rangle & \langle a^\dagger(t)a(t+\tau) \rangle \\ \langle a^\dagger(t+\tau)a(t) \rangle & \langle a^\dagger(t+\tau)a^\dagger(t) \rangle \end{pmatrix} : d\tau. \quad (18)$$

This matrix relates the discrete modes inside the cavity to the continuously distributed modes outside. The diagonal terms contain the information on phase-dependent aspects of the output field while the off-diagonal terms describe the ordinary amplitude-fluctuation spectrum.

In the Glauber-Sudarshan P representation this correlation matrix is given by the following correlation matrix of the c -number fields:

$$\underline{S}(\Omega) = \int e^{i\Omega\tau} \begin{pmatrix} \langle \alpha(t)\alpha(t+\tau) \rangle & \langle \alpha^*(t)\alpha(t+\tau) \rangle \\ \langle \alpha^*(t+\tau)\alpha(t) \rangle & \langle \alpha^*(t)\alpha^*(t+\tau) \rangle \end{pmatrix} d\tau.$$

In the case of interest here, the two-mode version of the c -number correlation matrix must be considered. This takes the form

$$\underline{S}(\Omega) = \int e^{i\Omega\tau} \begin{pmatrix} \langle \alpha_+(t)\alpha_+(t+\tau) \rangle & \langle \alpha_+^*(t)\alpha_+(t+\tau) \rangle & \langle \alpha_-(t)\alpha_+(t+\tau) \rangle & \langle \alpha_-^*(t)\alpha_+(t+\tau) \rangle \\ \langle \alpha_+(t)\alpha_+^*(t+\tau) \rangle & \langle \alpha_+^*(t)\alpha_+^*(t+\tau) \rangle & \langle \alpha_-(t)\alpha_+^*(t+\tau) \rangle & \langle \alpha_-^*(t)\alpha_+^*(t+\tau) \rangle \\ \langle \alpha_+(t)\alpha_-(t+\tau) \rangle & \langle \alpha_+^*(t)\alpha_-(t+\tau) \rangle & \langle \alpha_-(t)\alpha_-(t+\tau) \rangle & \langle \alpha_-^*(t)\alpha_-(t+\tau) \rangle \\ \langle \alpha_+(t)\alpha_-^*(t+\tau) \rangle & \langle \alpha_+^*(t)\alpha_-^*(t+\tau) \rangle & \langle \alpha_-(t)\alpha_-^*(t+\tau) \rangle & \langle \alpha_-^*(t)\alpha_-^*(t+\tau) \rangle \end{pmatrix} d\tau. \quad (19)$$

It has been previously shown that²⁰

$$\underline{S}(\Omega) = (\underline{A} + i\Omega\underline{1})^{-1} \underline{D} (\underline{A}^T - i\Omega\underline{1})^{-1}, \quad (20)$$

where the frequency argument $\Omega = \Omega_N - m\Omega_c$ is the difference between the detected noise frequency and a multiple of the free spectral range of the empty (undressed) cavity. The steady-state solution of Eq. (15) is $\alpha = 0$. Thus only the deviations from the steady-state solution play any roll in what follows.

D. Detection

In heterodyne and homodyne detection of squeezed states produced by nondegenerate mixing processes, the electronic noise produced by the detector corresponds to a superposition of the nonlinearly coupled modes.^{1,4,6,22-24} Following the treatment of Ref. 4 we calculate the squeezing in the combinations

$$\begin{aligned} c &= \frac{1}{2}(a_+ + a_-), \\ d &= \frac{1}{2}(a_+ - a_-). \end{aligned} \quad (21)$$

The corresponding spectral matrix is given by

$$\tilde{\underline{S}}(\Omega) = \underline{M}^{-1} \underline{S}(\Omega) \underline{M}, \quad (22)$$

where

$$\begin{aligned} I_N(t) &= \sqrt{(c/4\pi)(\hbar\omega/V_Q)} \int_0^{\Delta\Omega_N} [E_{LO}^* e^{i\omega_p t} (a_S e^{-i\omega_S t} + a_I e^{-i\omega_I t}) + E_{LO} e^{-i\omega_p t} (a_S^\dagger e^{i\omega_S t} + a_I^\dagger e^{i\omega_I t})] d\Omega_N \\ &\equiv \int_0^{\Delta\Omega_N} [I(\Omega_N) e^{-i\Omega_N t} + \text{H.c.}] d\Omega_N, \end{aligned} \quad (26a)$$

where a_s and a_I are the free space modes at frequencies ω_S and ω_I , $\omega_S + \omega_I = 2\omega_p$, $\omega_S - \omega_p = \omega_p - \omega_I = \Omega_N$, and the integral is over the noise frequency bandwidth of interest, $\Delta\Omega_N$. The operator for the Fourier component of the noise at frequency Ω_N is

$$I(\Omega_N) = |E_{LO}| \sqrt{(c/4\pi)(\hbar\omega/V_Q)} [\cos\theta(a_S + a_I^\dagger) - i \sin\theta(a_S - a_I^\dagger)]. \quad (26b)$$

The noise detected by the spectrum analyzer at a frequency shift Ω_N is related to $\langle |I(\Omega_N)|^2 \rangle$.^{4,6,24} As Schumaker and Caves have shown,^{24,25} for coherent-state inputs, the fiber output has time stationary quadrature phase (TSQP) noise. In such a case, the information in the real and imaginary parts of $I(\Omega_N)$ is redundant and it is equivalent to study the variance of the field components described by the combination operator

$$\frac{1}{2}(a_s + a_I).$$

In the present cavity case, we must relate the modes c and

$$\underline{M} = \frac{1}{2} \begin{pmatrix} 1 & 0 & 1 & 0 \\ 0 & 1 & 0 & 1 \\ 1 & 0 & -1 & 0 \\ 0 & 1 & 0 & -1 \end{pmatrix}. \quad (23)$$

The matrix elements for the c mode are then

$$\begin{aligned} \tilde{S}_{11}(\Omega) &= \frac{-2i\chi\tilde{I}_c}{|G(\Omega)|^2} [2\kappa^2 - G + \Omega^2 - 2i\kappa(\Delta_p + 4\chi\tilde{I}_c)], \\ \tilde{S}_{22}(\Omega) &= \tilde{S}_{11}^*(\Omega), \end{aligned} \quad (24)$$

$$\tilde{S}_{12}(\Omega) = \tilde{S}_{21}(\Omega) = \frac{8\chi^2\tilde{I}_c\kappa}{|G(\Omega)|^2},$$

where

$$G = \kappa^2 + \Delta_p^2 + 8\chi\Delta_p\tilde{I}_c + 12\chi^2\tilde{I}_c^2 \quad \text{and} \quad (25)$$

$$|G(\Omega)|^2 = (G - \Omega^2)^2 + 4\Omega^2\kappa^2.$$

To detect the phase-dependent noise that is the signature of a squeezed state, one must mix the output waves from the fiber ring cavity with a local oscillator wave.^{1,4,6,22-24} The phase of the local oscillator is locked to that of the pump wave, with relative phase difference θ . As was shown in Ref. 4, fluctuations of the intensity at the detector are given by the beat terms between the local oscillator and the sidebands, as described by the operator:

d to the free space modes reaching the detector. This question has been addressed by Collett and Gardiner⁷ and by Collett and Walls⁹ who showed that the analogous variance is

$$\begin{aligned} V(\theta, \Omega_N, \Delta_p, \tilde{I}_c) &= \frac{1}{4} + \frac{\kappa_{\text{out}}}{2} [e^{-2i\theta} \tilde{S}_{11}(\Omega_N - m\Omega_c) \\ &\quad + e^{2i\theta} \tilde{S}_{22}(\Omega_N - m\Omega_c) + \tilde{S}_{21}(\Omega_N - m\Omega_c) \\ &\quad + \tilde{S}_{12}(\Omega_N - m\Omega_c)], \end{aligned} \quad (27)$$

where κ_{out} is the damping of the cavity due solely to the output coupling through the port at which squeezing is being detected, in the case of our interferometer

$$\kappa_{\text{out}} = \frac{\xi}{2} = \frac{\xi}{\xi + \epsilon} \kappa.$$

The phase angle θ is defined with respect to the input pump field E_p^a . In our proposed experiments, the heterodyne detection of the fluctuations in the field amplitude is accomplished by mixing these fluctuations with a local oscillator derived from the wave at frequency ω_p that exists through port d . The phase of the output wave at ω_p (relative to the input wave E_p^a) is obtained from Eq. (4)

$$\Phi_d = \arctan \left[\frac{-\xi \Delta_p}{\Delta_p^2 + (\epsilon^2 - \xi^2)/2} \right]$$

and the phase θ in Eq. (27) is varied experimentally by adjusting an external resonator phase Φ_x : $\theta = \Phi_x + \Phi_d$ (Refs. 9 and 10) (see Sec. IV A). The noise spectral density of the electrical power is

$$N(\theta, \Omega_N, \Delta_p, \tilde{I}_c) = R \frac{4e^2}{\hbar\omega} \frac{c}{nl} AI_{\text{LO}} V(\theta, \Omega_N, \Delta_p, \tilde{I}_c). \quad (28)$$

The factor c/nl is the intrinsic bandwidth due to the propagation time around the resonator, R is the electrical resistance, and $I_{\text{LO}}A$ is the local oscillator power. For coherent states at the sideband frequencies

$$V(\theta, \Omega_N, \Delta_p, \tilde{I}_c) = \frac{1}{4}, \quad (29)$$

$$N(\theta, \Omega_N, \Delta_p, \tilde{I}_c) = R \frac{e^2 c}{\hbar\omega nl} AI_{\text{LO}}. \quad (30)$$

Squeezing occurs whenever the variance in Eq. (27) or the noise in Eq. (28) falls below these values.

E. Special cases

Case I: Maximum circulating pump

A relatively simple case corresponds to having the maximum pump power circulating in the ring cavity and detecting noise near a multiple of the cavity-free spectral-range frequency. Bistability does not complicate this case as there always exists a unique condition that maximizes the circulating pump power. The maximum \tilde{I}_c condition implies a pump detuning and output phase of

$$\Delta_p = -2\chi\tilde{I}_c \text{ and } \Phi_d = 0.$$

This condition implies $G = \kappa^2$. Nevertheless, the increased pump power and cavity resonant enhancement of the sidebands improves the squeezing over the traveling wave case. Assuming $L = \epsilon = 0$,

$$\tilde{I}_c = |\tilde{E}_p^c|^2 = \frac{2\Omega_c}{\pi\xi} |\tilde{E}_p^a|^2, \quad (31)$$

we find that the variance becomes

$$\begin{aligned} V(\theta, \Omega + m\Omega_c, -2\chi\tilde{I}_c, \tilde{I}_c) \\ = \frac{1}{4} \{ [1 - 2r_{\text{eff}}(\Omega)\sin(2\theta) + 2r_{\text{eff}}^2(\Omega)(1 - \cos(2\theta))] \}, \end{aligned} \quad (32)$$

where

$$r_{\text{eff}}(\Omega) = \frac{4\chi\tilde{I}_c\kappa}{\kappa^2 + \Omega^2} \rightarrow \frac{2\Omega_c}{\pi\xi} r_c \text{ as } \Omega \rightarrow 0. \quad (33)$$

This is similar to the traveling-wave case except for the enhancement of the value of r_c . A plot of the minimum and maximum values for $V(\theta, m\Omega_c, -2\chi\tilde{I}_c, \tilde{I}_c)$ appears in Fig. 3. For feasible values of $\eta = 0.8$ the enhancement $2\Omega_c/\pi\xi$ is a factor of 20. In addition $\tilde{I}_c = 20|\tilde{E}_p^a|^2$, compared to the traveling-wave case where $\tilde{I}_c = |\tilde{E}_p^c|^2 = |\tilde{E}_p^a|^2$. Thus at constant input power, a ring interferometer of length l shows an effective squeeze parameter $(2\Omega_c/\pi\xi)^2$ larger than the same fiber used on the traveling-wave case. For $\eta = 0.8$, $(2\Omega_c/\pi\xi)^2 = 400$. A full treatment of this case using the Airy functions gives similar enhancements even for relatively small η . In the limit $\gamma = 1$, $\eta \rightarrow 0$, $\kappa \rightarrow \Omega_c/\pi$, and $\Omega \ll \kappa$, the traveling-wave case of Ref. 10 is recovered.

Case II: Pump mode becomes bistable

We now consider the case where the external pump field is detuned by an amount Δ_p from the cavity resonance. As the pump intensity is increased the output from the cavity at the central cavity resonance will undergo dispersive bistability. This is described by the state Eq. (9) the stable sections of which are plotted in Fig. 4(b). The turning points of this curve are given by

$$G = \kappa^2 + \Delta_p^2 + 8\chi\Delta_p\tilde{I}_c + 12\chi^2\tilde{I}_c^2 = 0. \quad (34)$$

The squeezing in the pumped cavity mode has recently been shown to be a maximum near the turning points.^{9,26} We now shall investigate the squeezing in the sideband

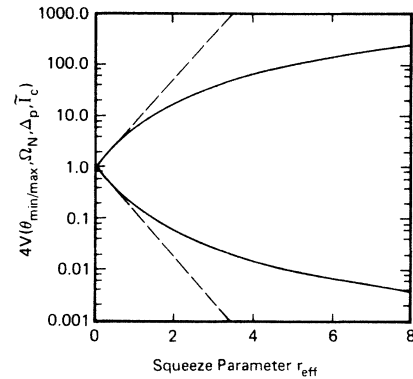


FIG. 3. Quantum noise variance as a function of effective squeeze parameter for the maximum circulating power case. The noise variance at the phase angles for maximum and minimum noise according to Eq. (32) is plotted as a solid line. The corresponding variances for the theory of Ref. 4 (where nonlinear dispersion was neglected) are plotted as dashed lines. For $r_{\text{eff}} > 0.5$, nonlinear dispersion significantly reduces the squeezing.

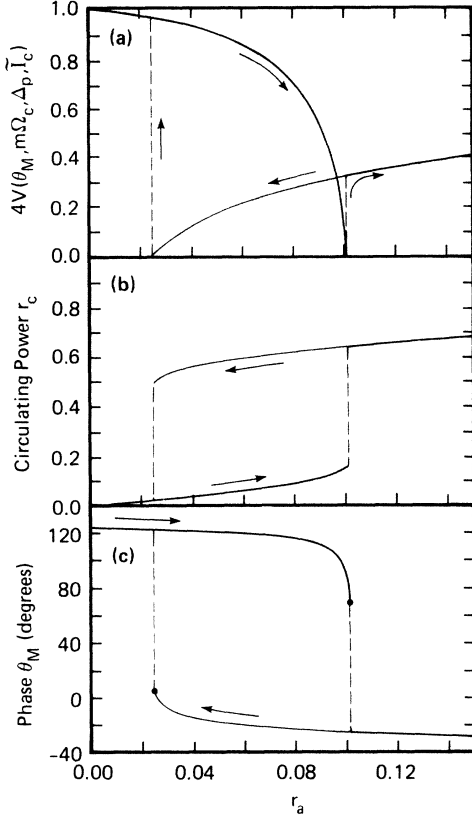


FIG. 4. Minimum quantum noise variance (a), circulating pump power (b), and phase (c) for maximum squeezing in the case where the circulating pump power is bistable. All curves are plotted as a function of the input beam squeeze parameter r_a , which parametrizes the input power. The heavy and light lines on each graph correspond to one another, and the dashed lines indicate discontinuities. The phases at the critical points are indicated by dots. All curves correspond to $\eta=0.8$ and $\Delta_p = -\Omega_c/4\pi$. Perfect squeezing of quantum noise is predicted for the critical points. The horizontal axis for all the curves is the input squeeze parameter r_a .

modes as the central mode intensity approaches bistable behavior. The squeezing spectrum is given by Eq. (27). We may choose the phase θ such that the squeezing is maximized at $\Omega_N = m\Omega_c$. The optimum choice of θ is then

$$e^{2i\theta_M} = \frac{\tilde{S}_{11}(0)}{|\tilde{S}_{11}(0)|} = \frac{-i[2\kappa^2 - G - 2i\kappa(\Delta_p + 4\chi\tilde{I}_c)]}{|2\kappa^2 - G - 2i\kappa(\Delta_p + 4\chi\tilde{I}_c)|}. \quad (35)$$

Assuming $\gamma=1$, this gives the variance

$$V(\theta_M, \Omega + m\Omega_c, \Delta_p, \tilde{I}_c) = \frac{1}{4} - \frac{\kappa\chi\tilde{I}_c}{|G(\Omega)|^2} \left[\left| \frac{2\kappa^2 - G + 2i\kappa(\Delta_p + 4\chi\tilde{I}_c)}{2\kappa^2 - G - 2i\kappa(\Delta_p + 4\chi\tilde{I}_c)} \right| \times [2\kappa^2 - (G - \Omega^2) - 2i\kappa(\Delta_p + 4\chi\tilde{I}_c)] + \text{c.c.} \right] - 8\chi\tilde{I}_c\kappa. \quad (36)$$

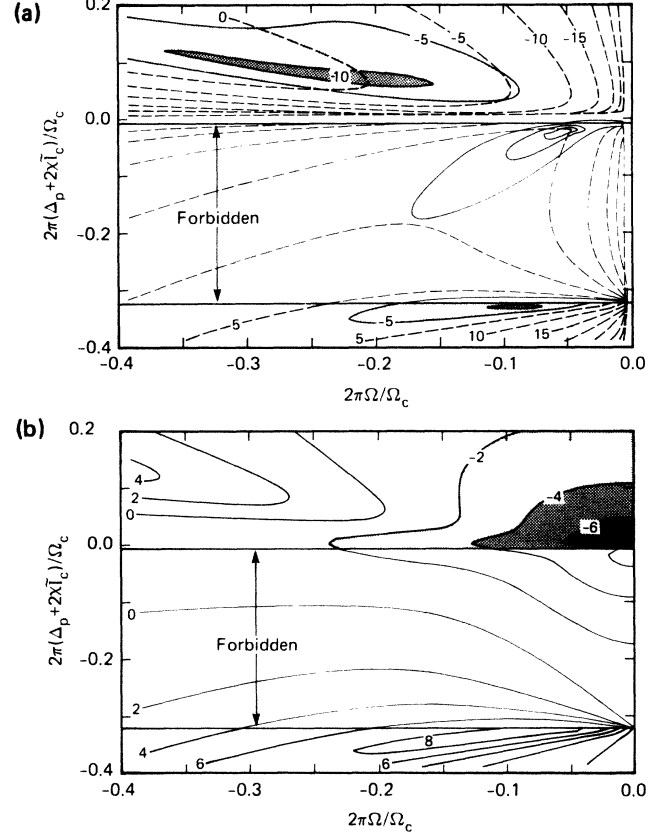


FIG. 5. (a) Contour map of quantum squeezing and GAWBS noise for the bistable case. The phase angle has been chosen to minimize the GAWBS noise as in Eq. (58). The horizontal axis represents the deviation frequency of the noise (as measured on the spectrum analyzer) from $m\Omega_c$. The map has mirror symmetry around $\Omega=0$. The vertical axis represents the frequency shift of the pump laser from the pumped cavity mode as shifted by the optical nonlinearity. Both axes are normalized to the resonator mode spacing $\Omega_c/2\pi$. The dashed lines show the GAWBS noise levels in steps of five decibels from the maximum noise level in a traveling-wave experiment with a similar fiber. These GAWBS contours depend on the value of β . The numbers indicate the noise levels of significant contours. Zero GAWBS noise (i.e., $-\infty$ dB) occurs for $\Omega=0$ and $\Delta_p + 2\chi\tilde{I}_c=0$. The shaded regions are areas where the quantum noise is below the coherent state limit. Again, numbers indicate the suppression in decibels. The forbidden region corresponds to the unstable branch of the bistability state equation. In this figure, the pump detuning is $\Delta_p = -\Omega_c/4\pi$ and the cavity decay rate is $\kappa=0.1$ ($\Omega_c/2\pi$). Quantum squeezing can only be detected when the GAWBS noise is very low. The most promising regions are in the upper left of the figure where significant squeezing is predicted only for $\Omega \approx 0.20$ ($\Omega_c/2\pi$). (b) Contour plot of the sum of the GAWBS and quantum noise at the phase of the minimum of the sum as functions of frequency and pump detuning. The axes are the same as in (a) and the numbers on the contours label the noise level in decibels with respect to the coherent-state limit. In the shaded region the total noise level is below the ordinary quantum limit. For this plot, the GAWBS parameter β was set equal to 5χ . Different ratios of β and χ yield qualitatively similar plots so long as β is less than about 50χ . The best lowest total noise occurs near the point of maximum circulating power and $\Omega=0$. As in (a), $\Delta_p = -\Omega_c/4\pi$ and $\kappa=0.1$ ($\Omega_c/2\pi$).

The maximum squeezing is found at the critical points $G=0$ where we find

$$V(\theta_M, \Omega + m\Omega_c, \Delta_{pM}) = \frac{1}{4} - \frac{\kappa^2}{4(\kappa^2 + \Omega^2)}, \quad (37)$$

which gives a value of zero at $\Omega=0$. The conjugate quadrature at $\theta_M + \pi/2$ has a corresponding divergence in fluctuations as the critical point is approached. Figure 4(a) shows the resulting dependence of the variance at the phase of minimum noise. The circulating pump power is shown in Fig. 4(b) as a function of the input pump. Very small values of the variance are experimentally accessible just below or just above the two critical points. The phase of the minimum variance is plotted in Fig. 4(c).

In Sec. IV of this paper, we will show that the effect of GAWBS noise can be minimized at certain phase shifts θ . When the pump is at resonance with a cavity mode, the minimum GAWBS phase shift is zero degrees, and no squeezing can be detected free from GAWBS interference. Likewise, when $\Omega_N = m\Omega_c$, minimum GAWBS phase generally corresponds to no squeezing. When the pump is detuned slightly from the cavity $\Delta_p \neq 0$ and $\Omega_N - m\Omega_c$ is nonzero, significant squeezing can be detected at a GAWBS minimum condition. Figure 5(a) shows contours of quantum noise variance at minimum GAWBS phase (solid lines) and GAWBS noise variance (dashed lines) as a function of the pump offset and fluctuation frequency. A quantum variance below 0.1 of the coherent state value can be obtained at this GAWBS minimum condition.

However, the best squeezing occurs near the bistability critical points where the GAWBS variance diverges, even at minimum GAWBS phase (see below). Therefore, we consider the total noise variance, quantum plus GAWBS, for a GAWBS scattering cross section typical for our fibers.¹² Contours of minima of this total noise variance are plotted in Fig. 5(b). Values a factor of 4 below that for a coherent state can still be obtained for this case. The best region is near zero pump offset ($\Delta_p + 2\chi\tilde{I}_c \approx 0$).

III. SUPPRESSING STIMULATED BRILLOUIN SCATTERING (SBS)

The nonlinear optical phenomenon with the lowest threshold is the stimulated Brillouin effect which reflects the pump light back down the fiber but with a frequency shift of roughly 1 cm^{-1} .¹¹ This stimulated scattering depletes the pump, clamps its power near the SBS threshold, and prevents the onset of other nonlinearities. To detect squeezing, the SBS threshold must be raised by at least a factor of 4.⁴

One of the early uses of the fiber-optic ring resonator was as an SBS oscillator. When the resonator damping rate is sufficiently low, the SBS threshold corresponds to an input pump power of less than 1 mW.¹⁴ The Brillouin light circulates around the ring in the opposite direction to the pump, and both frequencies lie at cavity resonances. This SBS oscillation must be totally suppressed if squeezing is to be detected, and it must be suppressed without increasing the damping rate for radiation circulating in the forward direction.

In the proposed experiments to generate squeezed states using a traveling-wave fiber geometry, a large temperature

gradient was suggested as a means of broadening the SBS gain line and reducing its maximum.^{4,10} While this method does work, it is not suitable for use in a ring resonator which must have a stable optical length. The fluctuations in temperature that seem inevitable with a large temperature gradient cause undesirable jitter in the cavity-resonant frequencies. Stable operation of a ring resonator requires a well stabilized average temperature, isolation from acoustic vibrations as well as servo control of the cavity length.¹⁵

The problem of suppressing the backwards SBS oscillation in a fiber ring cavity is similar to the problem of maintaining unidirectional oscillation in a ring-type dye laser.²⁷ In each case an optical diode consisting of a Faraday rotator, birefringent rotator plate, and a polarization selective element can induce loss for polarized light propagating in only one direction. The polarization rotating effects of the Faraday rotator and birefringent plate add for light propagating backwards, but cancel for light propagating in the forward direction. The elements of a fiber-optic diode have been demonstrated separately, and one might well expect that it is feasible to combine them in a single low-loss structure.²⁸⁻³¹

Suppressing SBS in a ring resonator requires much more asymmetry than maintaining unidirectional laser oscillation. In a laser, the gains in the forward and backwards direction are equal, and a few percent asymmetry is sufficient to stabilize the oscillation. In fibers, forward four-wave mixing never reaches threshold, and to reach a given value of r the backwards SBS wave must encounter a round trip attenuation greater than $\exp(-gn^2c^2r/48\pi f\chi^{(3)})$ where g is the SBS gain. Most of the optical fibers that are suitable for use with directional couplers also tend to randomize the polarization of the light propagating through them. Special low-birefringence spun fiber must be used in a ring resonator with an optical diode.²⁸

The overall scheme of our optical diode appears in Fig. 6. The Faraday rotator material is the fused silica of the fiber itself. Since the Verdet constant is small ($V_F = 3 \times 10^{-6} \text{ cm}^{-1} \text{ G}^{-1}$) and the maximum magnetic field in our solenoid electromagnet is 2 kG, considerable length of fiber is required for $\pi/4$ (45°) rotation. Rather than using a very long solenoid, we have followed Bergh in using ~ 20 10-cm straight lengths of fiber back and forth through the magnet with loops of fiber acting as half wave plates between.²⁹ The half wave plates reverse the angle between the planes of polarization and the plane of the loop, thereby allowing the Faraday rotations on successive passes through the magnet to add. When the half wave plates at each end of the magnet are at right angles to one another, the net linear birefringence of the Faraday rotator vanishes.

The wave plate which counters the Faraday rotation for forward propagating light consists of two loops of fiber in a circular slot. The plane of the slot could be pivoted around the fiber axis.³⁰ For a fiber of radius W the phase retardation induced by the stress birefringence of a single loop of radius R is

$$\Delta\Psi = 5.25 \frac{W^2}{R}.$$

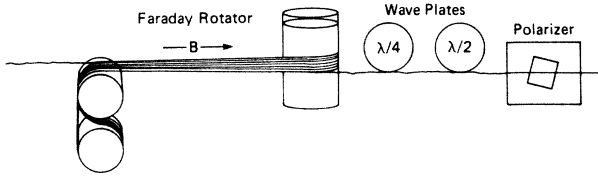


FIG. 6. Schematic of the optical diode. The 45° Faraday rotator consists of 10–24 straight segments of low-birefringence fiber in a magnetic field. A fiber half wave loop separates each such segment from the next and allows the Faraday rotations to add. A quarter wave plate insures that the output of the rotator is linearly polarized, and a half-wave loop oriented at 22.5° to the plane of polarization turns the forward propagating beam to its initial polarization condition. A polarizer consisting of a potassium pentaborate crystal contacted to half a directional coupler transmits the incident polarization while rejecting the orthogonal polarization. Such an optical diode can stabilize unidirectional propagation in a ring resonator with minimum insertion loss.

A quarter wave-plate loop similar to the half wave loop is used to cancel any residual birefringence. Our polarizer consists of half of an evanescent-wave (Stanford) coupler with a plate of potassium pentaborate contacted to it.³¹ The ordinary refractive index of this crystal is less than that of the core, while the extraordinary index is slightly higher. Thus one plane of polarization is coupled out of the fiber with high efficiency, while the orthogonal plane remains confined.

Such an optical diode has considerable optical length and Brillouin gain itself, in contrast to the essentially passive diodes used in dye lasers. Neglecting this internal gain, one can easily show that the loss coefficients for forward and backward propagation are

$$T_F = \frac{1}{2} T_x [1 + \cos 2(\Psi_F - \Psi_B) \cos \Psi_R] + \frac{1}{2} T_y [1 + \cos 2(\Psi_F + \Psi_B) \cos \Psi_R], \quad (38)$$

$$T_B = \frac{1}{2} T_x [1 + \cos 2(\Psi_B + \Psi_F) \cos \Psi_R] + \frac{1}{2} T_y [1 + \cos 2(\Psi_F - \Psi_B) \cos \Psi_R], \quad (39)$$

where Ψ_F is the Faraday rotation, Ψ_B is the rotation induced by the half wave plate, Ψ_R is the residual phase shift due to birefringence uncompensated by the quarter wave plate, and T_x and T_y are the transmission coefficients of the polarizer in the two orthogonal planes ($\Psi_R \ll \Psi_F \approx \Psi_B$ and $T_y \ll T_x$). The SBS threshold condition for a ring resonator containing such a diode and otherwise preserving polarization is then

$$\gamma_F \eta T_B e^{\tilde{g}_c l} \geq 1, \quad (40)$$

where \tilde{g}_c is the peak Brillouin gain, η is the coupler efficiency, γ_F is the transmission of the fiber and l is the length of the fiber in the cavity. For a silica fiber with core diameter $a = 3.5 \mu\text{m}$, the gain coefficient is $\tilde{g}_c = (3.1 \pm 0.6) \times 10^{-2} P_c \text{ cm}^{-1}$ where P_c is in watts.¹⁴

The transmission γ for forward-propagating waves in Eqs. (1) and (2) waves includes the diode forward

transmission loss T_F :

$$\gamma = \gamma_F T_F.$$

Clearly the insertion loss T_F for the optical diode can be less than $1 - \eta$.

Even with perfect diode rejection, the stimulated Brillouin effect can still cause superfluorescent oscillation in a single pass around the resonator. When $\tilde{g}_c l = 5$, this single-pass gain is sufficient to add measurable noise to the circulating pump.³² In practice, this limit can be approached with a diode, but not without. Higher pump powers are still possible, but not useful for squeezing. Without the diode, the oscillation threshold condition would be

$$\gamma \eta e^{\tilde{g}_c l} \geq 1. \quad (41)$$

Thus the feasible increase in circulating pump power when an optical diode is incorporated in a ring resonator is

$$\frac{\Delta \tilde{I}_c}{\tilde{I}_c} = (\log T_B / \log \gamma_F \eta). \quad (42)$$

The effect of the anisotropic SBS gain inside the optical diode can be modeled by noting that the polarization of the pump wave varies in a magnetic field as

$$\hat{\mathbf{p}} = \hat{\mathbf{x}} \cos \psi(z - z_0) - \hat{\mathbf{y}} \sin \psi(z - z_0), \quad (43)$$

where z_0 is the length of the magnetized region of the diode, $\psi z_0 = \Psi_F$ is the total Faraday rotation, the z axis is chosen in the SBS propagation direction, and the $\hat{\mathbf{x}}$ axis is the transmission axis of the polarizer. The wave equation for the SBS light has the form

$$\frac{\partial E_{Bx}}{\partial z} = \frac{\tilde{g}_c}{2} \cos^2 \psi(z - z_0) E_{Bx} + \left[\frac{\tilde{g}_c}{4} \sin(2\psi)(z - z_0) - \psi \right] E_{By}, \quad (44)$$

$$\frac{\partial E_{By}}{\partial z} = \left[\frac{\tilde{g}_c}{4} \sin(2\psi)(z - z_0) + \psi \right] E_{Bx} + \frac{\tilde{g}_c}{2} \sin^2 \psi(z - z_0) E_{By}. \quad (45)$$

The SBS light polarized in the x direction at $z = z_0$ is transmitted around the ring and is rotated by Ψ_B by the half wave plate so that the initial condition at $z = 0$ is

$$E_B(0) = E_B \hat{\mathbf{x}} \cos \Psi_B + E_B \hat{\mathbf{y}} \sin \Psi_B. \quad (46)$$

The condition for maximum transmission of the pump light is $\Psi_B = \Psi_F$, and if the internal gain were zero, the maximum rejection would occur for $\Psi_F = \pi/4$. Equations (44) and (45) can be solved for $\tilde{g}_c \neq 0$ by standard matrix techniques. The solutions where $\tilde{g}_c < 2\psi$ are relevant to this application, and $\Psi_B = \Psi_F$ will be assumed due to the need to maximize the pump transmission. We have performed the calculation and found that the effect of SBS gain in the diode is small. In particular when

$$\Psi_F \left[1 + \left[1 - \frac{g^2 \tilde{I}_c^2 z_0^2}{2\Psi_F^4} [1 - \cos(2\Psi_F)] \right]^{1/2} \right] = \frac{\pi}{2}, \quad (47)$$

$T_y=0$ and $\Psi_R=0$, the SBS power transmitted through the optical diode is

$$T_B = \frac{4g^6 \tilde{I}_c^6 z_0^6}{\pi^4 \Psi_F^6} e^{g\tilde{I}_c z_0}, \quad (48)$$

where z_0 is the optical length of the diode. Since $\Psi_F \approx \pi/4$ even in this case and $g^2 \tilde{I}_c^2 z_0^2 \ll 4\Psi_F^2$ this extra transmission is a negligibly small change, much less than that due to nonzero T_y and Ψ_R . We thus expect that sufficient SBS suppression for modest values of r_c can be achieved experimentally.

A. Faraday rotator demonstration

We were fortunate in obtaining a 6.7 m length of York LB600 low-birefringence spun fiber with attenuation below 20 dB/km, 3.5 μm core diameter and $W=46 \mu\text{m}$. The SBS threshold for such a fiber is above the power level that we can easily couple into this fiber. However, the SBS threshold of a ring fiber resonator is dramatically lower than that of a simple fiber, even if the return coupling of the resonator is quite low.³³ We have built such a resonator and incorporated an optical diode structure consisting of a Faraday rotator, wave plate, and polarizer within the loop. The coupler employed consisted of a pair of microscope objectives and a beam splitter as no evanescent wave coupler was available. The polarizer was a low-reflection coated Glan Thompson prism. The resulting resonator had relatively low finesse; however, we were able to show that the optical diode raised the SBS threshold without increasing the cavity loss or reducing the finesse.

The overall device appears in Fig. 7. A terbium-gallium-garnet Faraday rotator isolator decoupled the stabilized single-mode krypton-ion laser from the ring fiber resonator. The incident polarization was linear and vertical. Mode coupling was accomplished with auxiliary lenses and mirrors. The laser power was incident upon a 50% beam splitter; the transmitted portion was coupled into the fiber by a 20 \times microscope objective. The fiber then passed into the Faraday rotator which was constructed according to the design of Bergh and consisted of 20 straight lengths of fiber in a 1.2-kG magnetic field separated by 19 fiber half-wave plate loops that reversed the direction of the fiber.²⁹ The total length of fiber in the Faraday rotator assembly was ~ 4.8 m. After the rotator the fiber was wound six times around a piezoelectric transducer cylinder which could be used to vary the resonator frequency by stretching the fiber. After the piezo cylinder came a fiber quarter wave-plate which was adjusted to make the polarization linear at its output. A variable half-wave-plate fiber loop then oriented the transmitted linear polarization parallel to the incident polarization. The fiber output was recollimated by a second 20 \times microscope objective and passed through the Glan polarizer to be partly reflected by the beam splitter back

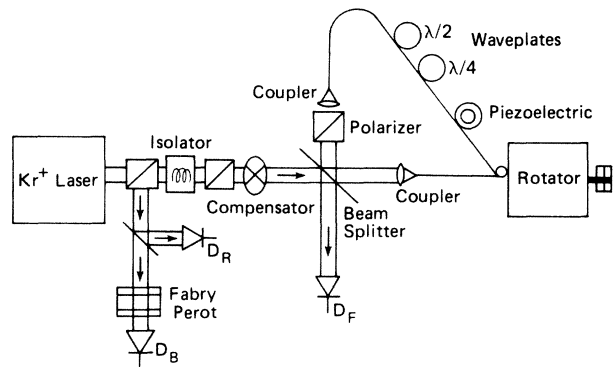


FIG. 7. Apparatus for testing the suppression of the stimulated Brillouin effect in a ring resonator. The resonator consists of a conventional beam splitter, two fiber coupling lenses and a length of fiber. A Glan Thompson polarizer rejects one plane of polarization. The fiber contains a Faraday rotator and retarder loops so that the polarization of light propagating in one direction remains undisturbed, while that propagating in the other direction is rotated by 90°. A piezoelectric cylinder scans the length of the resonator. The power of the light propagating in the forward direction is monitored by detector D_F , and backwards propagating light by detector D_R . Backwards propagating light shifted by the Brillouin frequency passes through the Fabry Perot interferometer and is detected at D_B . Because some light transmitted through (or reflected from) the beam splitter is not coupled into the fiber, the power at detector D_F does not go to zero even when the theoretical formula in Eq. (2) indicates that it should.

into the fiber loop and partly transmitted as output.

With the beam splitter misaligned, the magnetic field and phase-retarder loops could be adjusted to give perfect rejection (i.e., $T_B=0$). However, this condition required critical adjustment and the rejection varied with time, due possibly to temperature variation. For the present purposes, such a rejection measurement is less valuable than one where the cavity is correctly aligned.

In the cavity experiment, the piezotranslator was coupled to the horizontal axis of an oscilloscope. The signal from a photodiode monitoring the output of the resonator was displayed on one vertical axis of the three-beam oscilloscope while the other traces showed the power of the wave propagating around the loop in the opposite direction and the Brillouin shifted power. Below the SBS threshold, the backwards wave is due to reflections at interfaces within the loop and has the same frequency as the incident light. Above the SBS threshold, a new frequency component appeared which was resolved with a Fabry-Perot interferometer and displayed.

When the ring-resonator frequency equaled the incident laser frequency, the forward power was minimum, but not zero even when the loss inside the resonator (due to miscoupling, reflection loss, etc.) equaled the 40% input coupling. The oscilloscope trace labeled I_F in Fig. 8 shows the Airy function reflection characteristic of the optical resonator. The offset from zero is due mostly to poor input coupling from the laser. With zero magnetic field, the wave plates, beam splitter mirror, and micro-

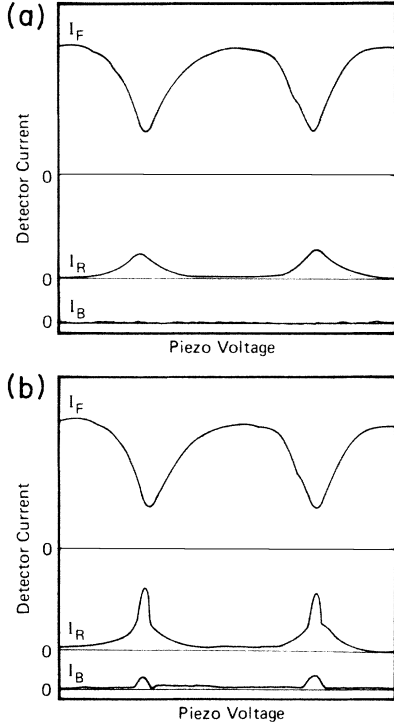


FIG. 8. (a) Detector signals from the apparatus of Fig. 7 for intensities below the stimulated Brillouin threshold. The intensity of the forward wave I_F is detected by the photodiode D_F and shows the expected Airy function profile as the ring-resonator length is scanned. The reflected intensity I_R is due to scattering by surfaces and parallels the circulating power. There is no light at the Brillouin-shifted frequency. (b) Detector signals from the apparatus of Fig. 7 for intensities above the stimulated Brillouin threshold. The forward propagating wave intensity I_F is not noticeably affected by the stimulated Brillouin effect, but the reflected intensity I_R shows sharp increases whenever the circulating pump power reaches a maximum. The intensity of the Brillouin-shifted component I_B is nonzero only when the spikes appear in the reflected signal. As the pump power is increased above threshold, the Brillouin pulses become wider.

scope objectives could be adjusted to give a cavity finesse of 4.1, consistent with expectations. The circulating pump power within the resonator is enhanced by a factor of 2.8 over the power coupled into the fiber when the beam splitter was misaligned. The relevant SBS threshold condition is in Eq. (41) where $\eta\gamma=0.16$. Because the initial coupling of the laser into the cavity is not optimum, the circulating power is less than the incident laser power. At a circulating power of 80 mW (and at an incident power of 250 mW), the power of the backwards-propagating wave increases discontinuously as shown in the middle trace of Fig. 8(b). This condition occurs only when the pump light and frequency shifted SBS light are simultaneously resonant with cavity modes and represents the minimum SBS threshold. The frequency shift of the excess reflected power was verified using a Fabry Perot and agreed with the theoretically expected shift of 1 cm^{-1} .

When the magnetic field was turned on, the reflection coefficient of the interferometer as a function of fiber length was dramatically altered. Additional peaks appeared in the reflection function due to interference between waves making multiple passes around the loop. Correctly adjusting the wave plates suppressed the additional peaks and restored the cavity finesse and minimum reflection coefficient. This adjustment required repeated realignment of the axes of the half and quarter wave plates to minimize the depolarization of the forward wave. When the finesse was 4.1 the SBS threshold obtained with optimum wave-plate adjustment and 45° Faraday rotation was an incident power of 840 mW or a circulating power of 280 mW.

The 3.5-fold increase in the threshold and Eq. (42) implies that the backwards transmission coefficient for this particular diode was $T_B=0.01$ limited—most likely—by stray birefringence. If the diode in our final resonator where $\eta\gamma=0.8$ has similar rejection, a circulating power of 92 mW should be possible with a 17-m optical length. Under the conditions leading to Eq. (33), the effective squeezing parameter would be $r_{\text{eff}}(0)=0.56$. The threshold for bistability in the $\eta\gamma=0.8$ resonator is $r_c=0.115$. Reaching that level would require an optical diode with $T_B \leq 1 \times 10^{-9}$, unless a temperature gradient or some other technique were found to reduce the SBS gain. Such a diode rejection does not seem feasible in the current design. In addition $r_c=0.115$ implies $g\tilde{I}_c l > 15$, well above the level where superfluorescent SBS noise overwhelms quantum noise. Thus one must seriously consider employing multiple SBS suppression methods in the bistable resonator. However, the exponential dependence of the required rejection upon gain and circulating power introduces considerable uncertainty in such estimates. Further experimental evidence is desirable.

IV. EFFECTS OF GUIDED ACOUSTIC WAVE BRILLOUIN SCATTERING IN THE RING CAVITY

Mechanical modes of vibration of the optical fiber will be thermally excited at room temperature. Some of these modes modulate the index of refraction at the fiber core, thereby phase modulating the pump beam.¹² At the high modulation frequencies typical of GAWBS additional noise is created at the frequencies of the sideband modes being squeezed. GAWBS is the bane of experiments to generate squeezed states in the traveling-wave fiber geometry. The thermal noise of GAWBS is many times the quantum level under typical experimental conditions, and is immune to the squeezing interaction. The only condition under which the GAWBS vanishes is at $\theta=0$, where squeezing also disappears at all finite pump intensities. One must hope that the case of the ring resonator is substantially different.

The mechanical modes of the fiber are best described as damped harmonic oscillators, with creation and destruction operators b_G^\dagger and b_G and frequencies Ω_G . The Hamiltonian which couples these modes to the sideband light-wave operators is

$$\mathcal{H}_G = \hbar(a_+^\dagger \tilde{E}_p + a_- \tilde{E}_p^*)B + \hbar(a_-^\dagger \tilde{E}_p + a_+ \tilde{E}_p^*)B^\dagger, \quad (49)$$

where

$$B^\dagger = \tilde{R} \sum_G b_G^\dagger, \quad B = \tilde{R}^* \sum_G b_G, \quad (50)$$

and \tilde{R} is a dimensional coupling constant. This Hamiltonian describes the physical process of coupled Stokes and anti-Stokes Brillouin scattering. The Stokes mode is a_- and anti-Stokes mode a_+ . The quantum theory of this process has been given by Walls³⁴ where the diffusion matrix is derived. We merely summarize the results here. Because of the interaction in Eq. (49), the equation of motion for the stochastic amplitude vector α [i.e., Eq. (15)] contains additional noise terms of the form

$$\left. \frac{\partial \alpha}{\partial t} \right|_G = \begin{pmatrix} -iB\tilde{E}_p \\ iB^\dagger \tilde{E}_p^* \\ -iB^\dagger \tilde{E}_p^* \\ iB\tilde{E}_p \end{pmatrix}. \quad (51)$$

While the fluctuating forces due to GAWBS have complex correlation properties which reflects the structure of the GAWBS spectrum, it suffices for the purpose of this derivation to treat them as describing a delta-correlated noise source. GAWBS contributes an additional term \underline{D}_G to the diffusion matrix given by³⁴

$$\underline{D}_G = \beta \tilde{I}_c \begin{pmatrix} 0 & 1 & -1 & 0 \\ 1 & 0 & 0 & -1 \\ -1 & 0 & 0 & 1 \\ 0 & -1 & 1 & 0 \end{pmatrix}, \quad (52)$$

which can be inserted into Eqs. (20) and (27) to obtain the GAWBS contributions to the S matrix and the variance. The temperature has been assumed much larger than $\hbar\Omega_G/k$ and terms of order $\hbar\Omega_G/kT$ have been dropped. All GAWBS contributions to the A matrix are neglected for this reason. However, any finite GAWBS contribution to A prevents the total suppression of quantum noise at the critical point. It will be apparent that this is not the most catastrophic effect of GAWBS noise in a fiber ring resonator. The full master-equation treatment yields the coefficient β in terms of the phonon density of states $\rho(\Omega_N)$ and \tilde{R} : $\beta = 2\pi\rho(\Omega_N) |\tilde{R}|^2 (kT/\hbar\Omega_G)$.

After some matrix algebraic manipulations, we find that

$$S_{11} = \frac{-2\beta\tilde{I}_c}{|G(\Omega)|^2} [\kappa^2 + \Omega^2 - (\Delta_p + 2\chi\tilde{I}_c)^2 - 2i\kappa(\Delta + 2\chi\tilde{I}_c)], \quad (53)$$

$$S_{22} = S_{11}^*, \quad (54)$$

$$S_{21} + S_{12} = \frac{4\beta\tilde{I}_c}{|G(\Omega)|^2} [\kappa^2 + \Omega^2 + (\Delta_p + 2\chi\tilde{I}_c)^2], \quad (55)$$

and

$$\begin{aligned} V_G(\theta, \Omega + m\Omega_c, \Delta_p, \tilde{I}_c) &= \frac{4\beta\tilde{I}_c\kappa}{|G(\Omega)|^2} \{ \kappa^2 + \Omega^2 + (\Delta_p + 2\chi\tilde{I}_c)^2 \\ &\quad - [\kappa^2 + \Omega^2 - (\Delta_p + 2\chi\tilde{I}_c)^2] \cos 2\theta \\ &\quad + 2\kappa(\Delta + 2\chi\tilde{I}_c) \sin 2\theta \}, \end{aligned} \quad (56)$$

where

$$\begin{aligned} |G(\Omega)|^2 &= (G - \Omega^2)^2 + 4\Omega^2\kappa^2, \\ G &= \kappa^2 + \Delta_p^2 + 8\chi\Delta_p\tilde{I}_c + 12\chi^2\tilde{I}_c^2, \end{aligned}$$

and $\Omega_N = \Omega + m\Omega_c$. This reduces to the functional form of the traveling-wave result when $\kappa^2 \gg \Omega^2, \chi\tilde{I}_c$.

Because the GAWBS effect is expected to be much larger than the quantum noise, it is particularly interesting to inquire under what circumstances $V_G = 0$. There are two such cases according to Eq. (56): $V_G = 0$ when $\Delta + 2\chi\tilde{I}_c = 0$ which corresponds to Case 1 of Sec. II A. The phase where $V_G = 0$ is, however, $\theta = 0$. Equation (32)—which gives the minimum variance—shows $V(0, \Omega_N, -2\chi\tilde{I}_c, \tilde{I}_c) = \frac{1}{4}$. Thus squeezing cannot be observed at this minimum in the GAWBS noise.

Another condition where GAWBS noise vanishes is $\Omega = 0$, which is also one of the conditions for perfect squeezing at the bistability critical points. The phase required to find this minimum in the GAWBS noise is

$$e^{-2i\theta_G} = \frac{\kappa^2 - (\Delta_p + 2\chi\tilde{I}_c)^2 + 2i\kappa(\Delta_p + 2\chi\tilde{I}_c)}{\kappa^2 + (\Delta_p + 2\chi\tilde{I}_c)^2}. \quad (57)$$

Equation (27) then gives the quantum noise variance at θ_G :

$$V(\theta_G, m\Omega_c, \Delta_p, \tilde{I}_c) = \frac{1}{4}.$$

Again the noise level is at the standard quantum limit independent of bistability.

Nonzero minimum GAWBS noise can be found for $\theta, \Delta_p + 2\chi\tilde{I}_c, \Omega \neq 0$. The phase angle for these minima is

$$e^{-2i\theta_{Gm}} = - \frac{(\Delta_p + 2\chi\tilde{I}_c)^2 - \kappa^2 - \Omega^2 - 2i\kappa(\Delta_p + 2\chi\tilde{I}_c)}{|(\Delta_p + 2\chi\tilde{I}_c)^2 - \kappa^2 - \Omega^2 - 2i\kappa(\Delta_p + 2\chi\tilde{I}_c)|}, \quad (58)$$

and the minimum GAWBS variance is

$$V_G(\theta_{Gm}, \Omega + m\Omega_c, \Delta_p, \tilde{I}_c) = \frac{4\beta\tilde{I}_c\kappa}{|G(\Omega)|^2} [\kappa^2 + (\Delta + 2\chi\tilde{I}_c)^2 + \Omega^2] \left[1 - \left[1 - \frac{4\Omega^2(\Delta + 2\chi\tilde{I}_c)^2}{[\kappa^2 + (\Delta_p + 2\chi\tilde{I}_c)^2 + \Omega^2]} \right]^{1/2} \right]. \quad (59)$$

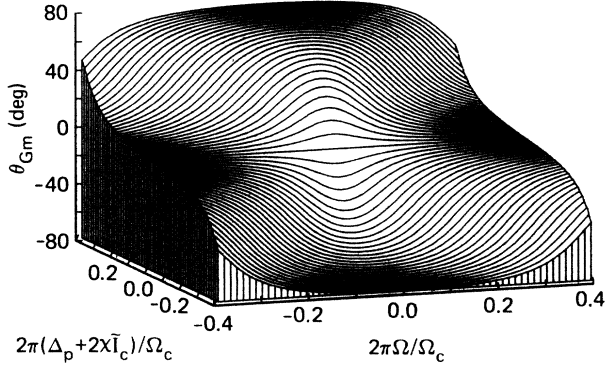


FIG. 9. The phase of the minimum GAWBS noise signal as a function of the detuning of the pump from the resonance of the cavity (as shifted by nonlinear effects) and the detuning of the noise frequency from the cavity-mode spacing. The horizontal axes are normalized to the resonator mode spacing $\Omega_c/2\pi$. When $\Omega=0$ or $\Delta_p + 2\chi\tilde{I}_c=0$, the minimum GAWBS noise is zero. The phase dependence is unaffected by bistability. The cavity decay rate is $\kappa=0.1(\Omega_c/2\pi)$.

Figures 9 and 10 plot the phase angle and magnitude of the minimum V_G as functions of Ω and $\Delta + 2\chi\tilde{I}_c$. The magnitude plot in Fig. 10 has been rescaled by $|G(\Omega)|^2$ to eliminate divergence near the critical point. At frequencies between the GAWBS resonances, such minima might be sufficiently below the quantum noise level that a squeezed state can be observed, but the details would depend on the characteristics of the fiber and resonator. In general, the measured noise signal corresponds to the total noise variance:

$$V_{\text{tot}} = V_{\text{quantum}} + \frac{\beta(\Omega_N)}{\beta} V_{\text{GAWBS}} \quad (60)$$

where the coefficient $\beta(\Omega_N)/\beta$ reflects the GAWBS spectrum of the fiber as measured outside the resonator. Con-

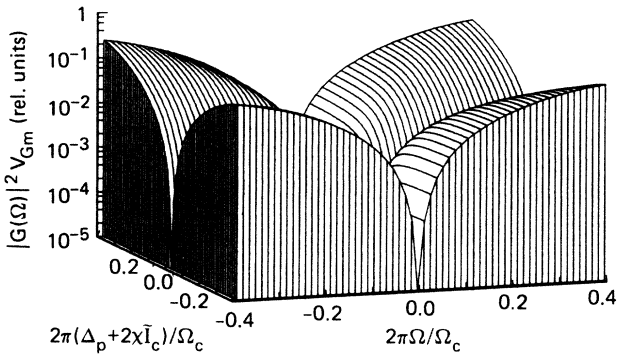


FIG. 10. The minimum GAWBS noise variance as a function of the pump detuning from the (shifted) resonance of the cavity and the noise frequency shift from the cavity-mode spacing. The horizontal axes have been normalized to the free spectral range of the cavity $\Omega_c/2\pi$. The GAWBS noise variance has been scaled by a factor $|G(\Omega)|^2$ which varies depending upon the distance of the operating point from the bistability critical points. The quantity plotted here is universal, applying to all operating points. The cavity decay rate is $\kappa=0.1(\Omega_c/2\pi)$.

tours of this total variance are plotted in Fig. 5(b) (see above). At bistability critical points $|G(0)|^2 \rightarrow 0$ and V_G diverges. Thus, for this reason alone, it will not be possible to observe the approach of perfect squeezing without some additional method for suppressing GAWBS.

An additional complexity is that some GAWBS modes cause depolarized scattering, thereby modulating both the polarization and phase of the light at the sideband frequencies. In the absence of a polarizer, the treatment above is sufficient to describe such modes, but our ring resonator will contain a polarization-selective element to suppress the stimulated Brillouin effect. When the polarization of the circulating pump light is not perfectly transmitted through the polarizer, that element can act to convert the polarization modulation into amplitude modulation.¹² Thus the depolarized GAWBS modes can contribute a term in the variance that does not vanish at $\theta=0$. The condition for minimizing this noise is also the condition for minimum cavity loss. The minimization of GAWBS at $\theta=0$ may be a sensitive means to optimize the cavity decay rate. The GAWBS noise remaining after optimization should vanish at some nonzero local oscillator phase. One may be justified in hoping that squeezing can be detected at such a minimum.

Special fibers have been designed which have very narrow GAWBS peaks with a few regions between them where the noise reaches the quantum limit.³⁵ Such fibers are at present too birefringent, too lossy, and too delicate for use in a ring resonator. Should it prove difficult to approach the bistability critical point, one might be forced to resort to such fibers in the future. Finally, cooling the entire resonator to liquid helium temperature should suppress the GAWBS noise by a factor of 60 or so, which would be sufficient to detect squeezing at most frequencies. Unfortunately, current resonator structures are incapable of operating at such low temperatures.

V. PROPOSED EXPERIMENT

A. Apparatus

The general scheme of our proposed method for generating and detecting squeezed states appears in Fig. 11. The output of a frequency-stabilized krypton-ion laser is passed through a Faraday rotation isolator and coupled into our ring fiber resonator. Obtaining sufficient frequency stability may require an external acousto-optic/electrooptic stabilizer of the sort demonstrated by Hansch and Hall.³⁶ The power level coupled into the fiber will be on the order of 10 mW, necessitating attenuation of the laser beam.

A low-birefringence optical fiber similar to York Technologies LB-600 spun fiber must be used, with attenuation below 12 dB/km and a jacket material giving GAWBS peaks as narrow as possible. At present, only acrylate jacket material is compatible with directional coupler technology. The fiber ring resonator will have 16–20 m total length. The input to the ring through the directional coupler will be variable, but anticipated to be 20%. Directly after the coupler, the light will pass through an

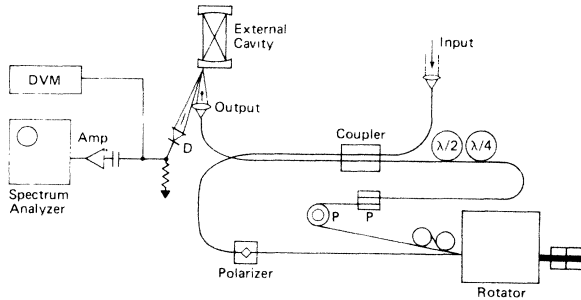


FIG. 11. Scheme of the proposed experiment to detect the generation of squeezed states of light by nondegenerate four-wave mixing in a fiber-optic ring resonator. The input light is focused into the resonator which contains a Faraday-rotator optical diode and piezoelectric transducers labeled *P*. These transducers are activated by servo electronics to maintain the correct operating point. The output of the ring resonator is reflected from an external cavity to phase shift the transmitted pump light. The resulting local oscillator wave and the noise amplitudes are converted into electrical signals by the photodiode *D*. A digital voltmeter labeled DVM measures the detector current by monitoring the potential developed on a load resistor. The ac components of the detector current are amplified and displayed on an electronic spectrum analyzer.

evanescent-wave polarizer with a rejection ratio above 1000:1.

After the polarizer, the fiber goes into our Faraday rotator which consists of 24 10-cm straight fiber segments inside the bore of a 1-kG solenoid. Between the fiber segments, the fiber direction is reversed by $\frac{1}{2}$ wave loops where the fiber is wrapped around two cylindrical drums 2.2 cm in diameter. The fiber does not go completely around either drum; rather the fiber is looped through a total angle of $\sim 420^\circ$ in a comma-shaped pattern. This allows precise adjustment of the phase retardation.

The fiber then coils 10 or more times around two 1-in.-diam piezoelectric cylinders with axes at right angles to one another to cancel the strain birefringence. These transducers alter the length of the optical path around the ring sufficiently to cancel detuning due to the anticipated 40-MHz frequency drift of the laser and can be changed rapidly enough to cancel jitter due to acoustic pickup. Following the transducers, the fiber passes through a $\frac{1}{4}$ wave loop 3.8 cm in diameter with variable orientation. This device cancels residual birefringence and makes the wave linearly polarized once more. A half wave plate similar to the preceding $\frac{1}{4}$ wave retarder, but with two loops, then returns the transmitted field to its initial polarization condition. The fiber then goes back into the directional coupler and from there to the output port.

The output of the fiber resonator is recollimated by a $20\times$ microscope objective and coupled into a ring interferometer made of discrete optical components. This device consists of two concave mirrors with 10-cm radius of curvature separated by 10 cm. The back mirror is coated for high reflectivity, while the front mirror has two coatings with different reflectivities. On the side of the mirror where the input beam is incident, the mirror transmis-

sion is finite, typically 3%. The other side of the mirror is coated for lower—perhaps zero—transmission. Such an interferometer has much of the alignment convenience of a confocal resonator. The phase of the reflected pump wave, however, varies with detuning from resonance over a full 360° when the loss due to the reflections other than that at the input (i.e., *L*) is less than the transmission at the input. Equation (2) describes the phase and amplitude of the reflected wave. In Ref. 10, it was shown that such an interferometer can attenuate the reflected pump wave as well as shift its phase. In the present application, the internal loss *L* can be minimized and the reflected power maintained nearly constant independent of pump detuning.

This external phase-shifting cavity shifts the phase of the transmitted pump radiation with respect to the phases of fields at neighboring fiber resonator modes. The free spectral range of our external cavity is 750 MHz and the linewidth 10 MHz. The resonant frequency of the phase-shifting cavity is maintained at a constant offset with respect to the pump frequency by means of a conventional servo system.¹⁰ The phase Φ_x of the phase-shifting cavity can be varied by altering this offset.

The beam reflected from the phase-shifting interferometer contains the local oscillator wave as well as many possible pairs of signal and idler frequencies. This beam is directed into a *p-i-n* photodiode in a special electronic circuit that minimizes the thermal noise at the frequency band where squeezing is expected. The ac portion of the photodiode signal is amplified and dispersed in an electronic spectrum analyzer. The dc current is measured to allow the standard quantum noise level to be calculated and compared with the noise measured on the spectrum analyzer. The noise level, dc current, phase-shifting cavity offset, laser power, fiber cavity setting, etc., are logged with an IBM personal computer.

The main difficulty anticipated is locking the frequency of the fiber interferometer to the laser frequency which may be fluctuating rapidly on a scale similar to the 200-kHz cavity linewidth. If the piezoelectric transducers are weakly driven at a few kilohertz, the resulting oscillation of the pump intensity appears on the dc output of the noise-measuring diode. That dither signal can then be detected by a lock-in amplifier and fed back into the fiber resonator servo system. To decouple this servo from the one controlling the phase-shifting cavity, one must normalize the ac dither signal to the dc detector current.

B. Procedure

The GAWBS spectrum of the fiber used in the interferometer will have been determined by conventional techniques.¹² The modifications of the GAWBS spectrum due to the cavity resonances predicted in Eq. (56) will be verified by setting the phase Φ_x to an appropriate value and dispersing the electrical noise on the photodiode using the spectrum analyzer. The best frequency for detecting squeezing would be near a minimum of the GAWBS spectrum and a resonance of the interferometer. Near such a minimum, one can perhaps find a phase shift that gives a GAWBS noise level below the coherent state quantum

noise level while permitting detectable squeezing.

One must expect that the detection of quantum squeezing will be as difficult with this device as with the traveling-wave technique of Ref. 4. It thus will be instructive to simulate quantum noise with electrooptic modulators as in Ref. 10. The randomly modulated beam would be coupled into the cavity along with the pump wave. The noise spectrum as modified by any nonlinear effects in the cavity would then appear on the spectrum analyzer. By varying the external phase shift, input laser power, and frequency difference between ring cavity resonance and pump laser, the variance formula in Eq. (27) can be verified. Of special interest would be a condition where this simulated quantum noise is suppressed and the GAWBS noise is below the coherent state limit.

Once these preliminary experiments have been performed, the classically modulated beam will be blocked and a suppression of the total noise measured on the spectrum analyzer will be sought. The coherent-state quantum limit level would be verified by illuminating the detector with sufficient thermal light to give the same dc current as measured in the squeezing experiment.³⁷

In the first series of measurements, we plan to operate near the condition of maximum circulating pump power. The variation in the noise would follow Eq. (32) in that case. We expect to be able to achieve a maximum effective squeeze parameter of $r_{\text{eff}}(0)=0.5$ with less than 5 mW of laser power coupled into the ring resonator.

If the SBS suppression can be made great enough, negative detuning of the ring-resonator frequency from the point of maximum circulating power will put the operating point on the upper circulating pump power branch of the bistable region of Fig. 4. The quantum noise variance at the optimum phase for squeezing would decrease towards zero as the critical point is approached from above. The GAWBS noise will not be zero at this phase, but might be low enough at some nearby phase to reveal some squeezing. In any case, it will be interesting to explore the dynamics of the ring resonator near this critical point.

VI. CONCLUSIONS

We have shown in this paper that forward four-wave mixing in a fiber-optic ring interferometer squeezes the vacuum fluctuations in frequency bands shifted from the pump by multiples of the interferometer free spectral range. For given input power, the squeezing obtained is dramatically larger than in the traveling-wave case. At the critical points for optical bistability, the quantum noise is predicted to disappear at the optimum local oscillator phase.

The main impediment to the operation of such a nonlinear device is the need to totally suppress the stimulated Brillouin effect. We have shown how this may be accomplished with a Faraday-rotator optical diode incorporated within the fiber itself. We have also presented experimental evidence that this strategy would meet with limited success. Greater suppression might be accomplished by imposing a limited temperature gradient along the fiber.

The excess noise due to forward Brillouin scattering by

guided acoustic waves does not disappear under any condition where squeezing can be detected. Noise minima were predicted which might prove low enough to detect squeezing when fiber parameters are favorable.

Finally, we have described experimental apparatus and procedures expected to verify the theoretical predictions and perhaps to detect squeezing. To a great extent, success is dependent on obtaining suitable optical fiber. Not only must the core be small enough to provide sufficient nonlinearity, the linear birefringence low enough to allow Faraday rotation, the loss minimal, and the stimulated Brillouin threshold high, but the GAWBS spectrum must have gaps where the noise level approaches the quantum limit. This latter requirement probably implies that the jacket material must be metal as the GAWBS broadening due to a polymer jacket may unduly increase the noise level in the gaps. At present no such fiber is available.

ACKNOWLEDGMENTS

The authors acknowledge valuable insights from Dr. Margaret Reid, Dr. Ralph Bergh, and Dr. Wayne Sorin. This was partly supported by the U.S. Office of Naval Research.

APPENDIX

In this appendix we present an alternate derivation of the major results of Sec. II, based on a simultaneous self-consistent solution of the equations for four-wave mixing in a fiber ring, closed with a directional coupler with variable intensity coupling coefficient η . We do not employ the Lorentzian approximation used in the main part of the paper, and although the results appear somewhat more complicated as a result, they give the squeezing for arbitrary pump detuning Δ_p , and noise frequency Ω_N . The effects of the round-trip loss $1-\gamma$ are included in the derivation of the bistable state equation for the pump, which is done classically, but the effects of loss on the squeezing is neglected, and we set $\gamma=1$ for the signal and idler fields.

The starting point for this treatment is the set of equations describing the fields at the output of the coupler in terms of the input fields, and the equations which describe the propagation of the fields from c to b (see Fig. 1). The coupler equations are

$$E^c = \sqrt{\gamma}(\sqrt{1-\eta}E^a - e^{i\phi_c}\sqrt{\eta}E^b), \quad (\text{A1})$$

$$E^d = \sqrt{\gamma}(e^{-i\phi_c}\sqrt{\eta}E^a + \sqrt{1-\eta}E^b), \quad (\text{A2})$$

where the phase shift ϕ_c due to the coupler has no effect on the final results except to shift the pump offset where resonance occurs. Henceforth we take $\phi_c = \pi$ which gives resonances at phase detuning values of $2n\pi$. As shown for the traveling-wave case in Ref. 4, slow variations of the pump phase can be shown to have no effect and will be ignored. The equations for propagation of the pump, signal, and idler fields in the fiber from c to b are

$$\frac{\partial E_P}{\partial z} = 2iK |E_P|^2 E_P, \quad (\text{A3})$$

$$\frac{\partial \hat{E}_I}{\partial z} = 4iK |E_P|^2 \hat{E}_I + 2iKE_P^2 \hat{E}_S^\dagger, \quad (\text{A4})$$

$$\frac{\partial \hat{E}_S^\dagger}{\partial z} = -4iK |E_P|^2 \hat{E}_S^\dagger - 2iKE_P^{*2} \hat{E}_I, \quad (\text{A5})$$

where the pump field will be treated classically, $K = (6\pi\omega/c) f\chi^{(3)}$, and the signal and idler fields are treated quantum mechanically, the symbols $\hat{E}_{I,S}$ denoting the appropriate quantum-mechanical operators. The terms in Eqs. (A3) to (A5) proportional to $|E_P|^2$ describe the intensity-dependent phase shifts of the various fields, and the other terms in Eqs. (A4) and (A5) describe the parametric four-wave-mixing interaction. The solution of these equations for the pump field gives the bistable state equation which is identical in form to Eq. (1), but with an intensity-dependent round-trip phase delay:

$$E_P^g = \frac{\sqrt{\gamma(1-\eta)} E_P^g}{1 - \sqrt{\gamma\eta} e^{i\Phi}}, \quad (\text{A6})$$

$$\frac{|E_P^g|^2}{|E_P^g|^2} = \frac{r_c}{r_a} = \frac{\gamma(1-\eta)}{1 + \gamma\eta - 2\sqrt{\gamma\eta}\cos\Phi}, \quad (\text{A7})$$

where r_c and r_a are defined as in Eq. (7), r_c/r_a is equal to the ratio of circulating to input pump intensity, and $\Phi = 2\pi\Delta_P/\Omega_c + r_c$. These equations correspond to Eqs. (8) and (9), and serve as bistability state equations. The critical points of the optical bistability occur when

$$\cos\Phi_{cr} - r_c \sin\Phi_{cr} = (1 + \gamma\eta)/(2\sqrt{\gamma\eta}). \quad (\text{A8})$$

The output pump field is given by

$$E_P^g = -\sqrt{\gamma\eta} E_P^g \left[1 - \frac{\sqrt{\gamma/\eta}(1-\eta)e^{i\Phi}}{1 - \sqrt{\gamma\eta}e^{i\Phi}} \right] \\ \equiv -\sqrt{\gamma\eta} \mathcal{F}_0 E_P^g. \quad (\text{A9})$$

The solutions of the propagation equations for the signal and idler are given in Ref. 10, and reproduced here

$$\hat{E}_I^b = e^{i(\Phi+\delta)} [(1+ir_c)\hat{E}_I^c + ir_c\hat{E}_S^{\dagger c}], \quad (\text{A10})$$

$$\hat{E}_S^{\dagger b} = e^{-i(\Phi-\delta)} [-ir_c\hat{E}_I^c + (1-ir_c)\hat{E}_S^{\dagger c}], \quad (\text{A11})$$

where $\delta = 2\pi\Omega_N/\Omega_c$. Combining these two equations with the coupler equations for the signal and idler fields and requiring self-consistency, one arrives at the steady-state solutions for the signal and idler fields circulating in the cavity and for the output fields:

$$\hat{E}_I^c = \frac{\sqrt{(1-\eta)}}{D} \{ [1 - (1-ir_c)\sqrt{\eta}e^{-i(\Phi-\delta)}] \hat{E}_I^a + (ir_c)\sqrt{\eta}e^{i(\Phi+\delta)} \hat{E}_S^{\dagger a} \}, \quad (\text{A12})$$

$$\hat{E}_S^{\dagger c} = \frac{\sqrt{(1-\eta)}}{D} \{ (-ir_c)\sqrt{\eta}e^{-i(\Phi-\delta)} \hat{E}_I^a + [1 - (1+ir_c)\sqrt{\eta}e^{i(\Phi+\delta)}] \hat{E}_S^{\dagger a} \}, \quad (\text{A13})$$

$$\hat{E}_I^g = -\sqrt{\eta} \left[\left[1 - \frac{\sqrt{1/\eta}(1-\eta)e^{i(\Phi+\delta)}(1+ir_c - \sqrt{\eta}e^{-i(\Phi-\delta)})}{D} \right] \hat{E}_I^a + \frac{\sqrt{1/\eta}(1-\eta)(ir_c)e^{i(\Phi+\delta)}}{D} \hat{E}_S^{\dagger a} \right] \\ \equiv -\sqrt{\eta} (\mathcal{F}_+ \hat{E}_I^a + \mathcal{G}_- \hat{E}_S^{\dagger a}) \quad (\text{A14})$$

$$\hat{E}_S^{\dagger g} = -\sqrt{\eta} \left[\frac{\sqrt{1/\eta}(1-\eta)(-ir_c)e^{-i(\Phi-\delta)}}{D} \hat{E}_I^a + \left[1 - \frac{\sqrt{1/\eta}(1-\eta)e^{-i(\Phi-\delta)}(1-ir_c - \sqrt{\eta}e^{i(\Phi+\delta)})}{D} \right] \hat{E}_S^{\dagger a} \right] \\ \equiv -\sqrt{\eta} (\mathcal{G}_+ \hat{E}_I^a + \mathcal{F}_- \hat{E}_S^{\dagger a}), \quad (\text{A15})$$

where

$$D = 1 + \eta e^{i2\delta} - 2\sqrt{\eta} e^{i\delta} (\cos\Phi - r_c \sin\Phi). \quad (\text{A16})$$

As described before, the output of the fiber ring is mixed with a local oscillator wave obtained by attenuating the pump output field by a factor T and phase shifting it by Φ_x (i.e., $E_{LO} = TE_P^g e^{i\Phi_x}$). When the signal and idler operators in Eq. (26) are replaced by the expressions for the fiber ring output fields, one obtains

$$I(\Omega_N) = \eta \left[\frac{c}{4\pi} \frac{\hbar\omega}{V_Q} \right]^{1/2} T E_P^g \\ \times \{ [\hat{E}_I^g (e^{i\Phi_x} \mathcal{F}_0 \mathcal{G}_+ + e^{-i\Phi_x} \mathcal{F}_0^* \mathcal{F}_+) \\ + \hat{E}_S^{\dagger g} (e^{i\Phi_x} \mathcal{F}_0 \mathcal{F}_- + e^{-i\Phi_x} \mathcal{F}_0^* \mathcal{G}_-)] + \text{H.c.} \}. \quad (\text{A17})$$

The corresponding variance becomes

$$V(\Phi_x, \Phi, \delta, r) = (\eta/8) \{ |\mathcal{F}_+|^2 + |\mathcal{F}_-|^2 + |\mathcal{G}_+|^2 + |\mathcal{G}_-|^2 - 2 \operatorname{Re}[e^{i2\theta}(\mathcal{G}_+\mathcal{F}_+^* + \mathcal{G}_-\mathcal{F}_-^*)] \}, \quad (\text{A18})$$

where $\theta = \Phi_x + \Theta$ and

$$\tan \Theta = \frac{\operatorname{Im}(\mathcal{F}_0)}{\operatorname{Re}(\mathcal{F}_0)} = \frac{(\sqrt{\gamma\eta} - \sqrt{\gamma/\eta})\sin\Phi}{1 + \gamma + (\sqrt{\gamma/\eta} + \sqrt{\gamma\eta})\cos\Phi} \quad (\text{A19})$$

is the phase shift of the pump output with respect to the pump input. The minimum of this variance with respect to the external phase shift Φ_x occurs when

$$e^{i2\theta} = \frac{(\mathcal{G}_+\mathcal{F}_+^* + \mathcal{G}_-\mathcal{F}_-^*)}{|\mathcal{G}_+\mathcal{F}_+^* + \mathcal{G}_-\mathcal{F}_-^*|}, \quad (\text{A20})$$

for which

$$V_{\min} = (\eta/8) (|\mathcal{F}_+|^2 + |\mathcal{F}_-|^2 + |\mathcal{G}_+|^2 + |\mathcal{G}_-|^2 - 2|\mathcal{G}_+\mathcal{F}_+^* + \mathcal{G}_-\mathcal{F}_-^*|). \quad (\text{A21})$$

This is plotted in Fig. 12 as a function of noise frequency Ω_N and offset Φ for intensities near the onset of bistability. The results given in Eqs. (A18) and (A21) are identical to those of Eqs. (27) and (36) when the loss and the coupling satisfy $(L = 1 - \gamma), (1 - \eta) \ll 1$ and both the pump frequency is near resonance (i.e., $\Delta_p + 2\chi\tilde{I}_c \lesssim \kappa$ or $\Phi \simeq 0$) and the noise frequency is near a multiple of the free spec-

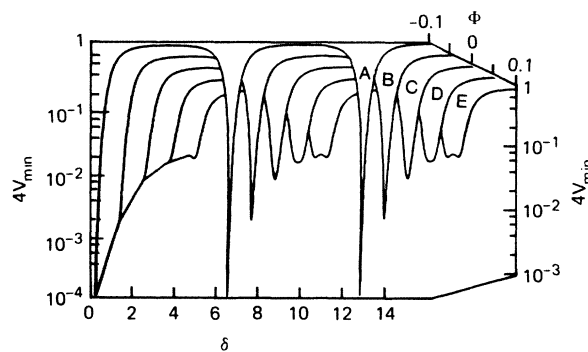


FIG. 12. The minimum quantum noise variance as in Eq. (A21) relative to that for a coherent state plotted as a function of the normalized noise frequency $\delta = 2\pi\Omega_N/\Omega_c$ and the offset of the pump frequency from its cavity mode as shifted by the nonlinear effects $\Phi = 2\pi\Delta_p/\Omega_c + r_c$. The noise minima at the first two ring-cavity resonances are shown as well as the minimum near $\delta = 0$ where the two sidebands and the pump all fall within the same resonance. In all these plots, $\Delta_p = -\Omega_c/4\pi$ and $\eta = 0.6$. Curve A corresponds to $r_c = 0.4$ and $r_a = 0.0585$, values very near a critical point for bistability. The minimum is thus very deep and narrow. Curve C at $\Phi = 0$ corresponds to the case of maximum circulating power ($r_c = 0.5$ and $r_a = 0.064$). The input and circulating powers for the other curves can be calculated from the Φ scale and the state equation, Eq. (A7).

tral range (i.e., $\Omega_N \simeq n\Omega_c$ or $\delta \simeq 2n\pi$).

For a given pump detuning and input intensity, the maximum squeezing occurs for exact sideband resonance, i.e., $\delta = 2n\pi$. For this condition one can show that Eq. (A18) reduces to

$$V^{\text{res}} = \left[\frac{1}{|D|^2} \right] (1 + 4\eta + \eta^2 + 2r_c^2(1 - \eta + \eta^2) - 4\sqrt{\eta}(1 + \eta)(\cos\Phi - r_c\sin\Phi) + 2\eta[(1 - r_c^2)\cos(2\Phi) - 2r_c\sin(2\Phi)] - 2r_c(1 - \eta) \{ \sin(2\theta) [-\cos(2\Phi) + r_c\sin(2\Phi) + 2\sqrt{\eta}\cos\Phi - \eta] + \cos(2\theta) [r_c\cos(2\Phi) + \sin(2\Phi) - 2\sqrt{\eta}\sin\Phi - \eta r_c] \}), \quad (\text{A22})$$

where $D = 1 + \eta - 2\sqrt{\eta}(\cos\Phi - r_c\sin\Phi)$. This takes on its minimum value when

$$\tan(2\theta) = \frac{[-\cos(2\Phi) + r_c\sin(2\Phi) + 2\sqrt{\eta}\cos\Phi - \eta]}{[r_c\cos(2\Phi) + \sin(2\Phi) - 2\sqrt{\eta}\sin\Phi - \eta r_c]}, \quad (\text{A23})$$

for which

$$V_{\min}^{\text{res}} = \left[\frac{1}{|D|^2} \right] (1 + 4\eta + \eta^2 + 2r_c^2(1 - \eta + \eta^2) - 4\sqrt{\eta}(1 + \eta)(\cos\Phi - r_c\sin\Phi) + 2\eta[(1 - r_c^2)\cos(2\Phi) - 2r_c\sin(2\Phi)] - 2r_c(1 - \eta) \{ (1 + r_c^2)(1 + \eta^2) + 4\eta - 4\sqrt{\eta}(1 + \eta)(\cos\Phi - r_c\sin\Phi) + 2\eta[(1 - r_c^2)\cos(2\Phi) - 2r_c\sin(2\Phi)] \}^{1/2}). \quad (\text{A24})$$

By inserting the condition for the bistability critical points [Eq. (A8)] one finds

$$V_{\min}^{\text{res}}(\Phi = \Phi_{cr}) = 0 \quad (\text{A25})$$

in agreement with the prediction of Eq. (37).

The condition of maximum circulating pump power discussed as Case 1 in Sec. IIE above corresponds to $\Phi = 0$. We then obtain from Eq. (A18)

$$V = \frac{1}{4} \{ 1 + 2r_{\text{eff}}(\delta)\sin(2\theta) + 2r_{\text{eff}}^2(\delta)[1 - \cos(2\theta)] \}, \quad (\text{A26})$$

where

$$r_{\text{eff}}(\delta) = r_c(1 - \eta)/(1 + \eta - 2\sqrt{\eta}\cos\delta). \quad (\text{A27})$$

For $\delta = 0$ we obtain

$$r_{\text{eff}}(0) = r_c \left[\frac{1 + \sqrt{\eta}}{1 - \sqrt{\eta}} \right] = r_a \left[\frac{1 + \sqrt{\eta}}{1 - \sqrt{\eta}} \right]^2 \approx r_a \left[\frac{2\Omega_c}{\xi\pi} \right]^2 \quad (\text{A28})$$

in agreement with Eq. (33) above. As $\eta \rightarrow 0$, $r_{\text{eff}}(0) \rightarrow r_a$ and we recover the traveling-wave result.¹⁰

*Permanent address: Physics Department, University of Waikato, Hamilton, New Zealand.

†Permanent address: Institut d'Optique Théorique et Appliquée, Centre Universitaire d'Orsay, Boîte Postale 43, 91406 Orsay, France.

¹For a review, see D. F. Walls, *Nature* (London) **306**, 141 (1983).

²R. S. Bondurant, P. Kumar, J. H. Shapiro, and M. Maeda, *Phys. Rev. A* **30**, 343 (1984).

³R. E. Slusher, L. Hollberg, B. Yurke, J. C. Mertz, and J. F. Valley, *Phys. Rev. A* **31**, 3512 (1985).

⁴M. D. Levenson, R. M. Shelby, M. D. Reid, D. F. Walls, and A. Aspect, *Phys. Rev. A* **32**, 1550 (1985).

⁵B. Yurke, *Phys. Rev. A* **29**, 408 (1984).

⁶B. Yurke, *Phys. Rev. A* **32**, 300 (1985).

⁷M. J. Collett and C. W. Gardiner, *Phys. Rev. A* **30**, 1386 (1984).

⁸M. D. Reid and D. F. Walls, *Phys. Rev. A* **31**, 1622 (1985).

⁹M. J. Collett and D. F. Walls, *Phys. Rev. A* **32**, 2887 (1985).

¹⁰M. D. Levenson, R. M. Shelby, and S. H. Perlmutter, *Opt. Lett.* **10**, 514 (1985).

¹¹E. P. Ippen and R. H. Stolen, *Appl. Phys. Lett.* **21**, 539 (1972).

¹²R. M. Shelby, M. D. Levenson, and P. W. Bayer, *Phys. Rev. B* **31**, 5244 (1985).

¹³L. F. Stokes, M. Chodorow, and H. J. Shaw, *Opt. Lett.* **7**, 288 (1982).

¹⁴L. F. Stokes, M. Chodorow, and H. J. Shaw, *Opt. Lett.* **7**, 509 (1982).

¹⁵L. F. Stokes, M. Chodorow, and H. J. Shaw, *IEEE J. Lightwave Technol.* **LT-1**, 110 (1983).

¹⁶M. Born and E. Wolf, *Principles of Optics*, 3rd revised ed. (Pergamon, Oxford, 1965), Sec. 7.6.

¹⁷M. D. Levenson, *Introduction to Nonlinear Laser Spectroscopy* (Academic, New York, 1982), Chap. 4.

¹⁸Y. R. Shen, *Principles of Nonlinear Optics* (Wiley, New York, 1984), Chap. 26.

¹⁹L. A. Lugiato, *Progress in Optics*, edited by E. Wolf (North-Holland, Amsterdam, 1984), Vol. XXI.

²⁰C. W. Gardiner, *Handbook of Stochastic Methods* (Springer, Berlin, 1983).

²¹P. D. Drummond and C. W. Gardiner, *J. Phys. A* **13**, 2353 (1980).

²²H. P. Yuen and J. H. Shapiro, *IEEE Trans. Inf. Theor.* **IT-26**, 78 (1980).

²³B. L. Schumaker, *Opt. Lett.* **9**, 189 (1984).

²⁴C. M. Caves and B. L. Schumaker, *Phys. Rev. A* **31**, 3068 (1985).

²⁵B. L. Schumaker, *Phys. Rep.* (to be published).

²⁶M. D. Reid and D. F. Walls, *Phys. Rev. A* **32**, 396 (1985).

²⁷S. M. Jarrett and J. F. Young, *Opt. Lett.* **4**, 176 (1979).

²⁸A. J. Barlow, J. J. Ranshov-Hansen and D. M. Payne, *Appl. Opt.* **20**, 2962 (1981).

²⁹R. A. Bergh, H. C. Lefevre, and H. J. Shaw, in *Fiber Optic Rotation Sensors and Related Technologies*, Vol. 32 of *Springer Series in Optical Sciences*, edited by S. Ezekiel and H. J. Arditty (Springer-Verlag, New York, 1982), pp. 400–405.

³⁰H. C. Lefevre and H. J. Shaw, *Electron Lett.* **14**, 778 (1980).

³¹R. A. Bergh, H. C. Lefevre, and H. J. Shaw, *Opt. Lett.* **5**, 479 (1980).

³²I. Bar-Joseph, A. A. Friesen, E. Lightman, and R. G. Waarts, paper presented at the Conference on Lasers and Electro Optics, Baltimore, 1985 (unpublished).

³³D. R. Ponikvar and S. Ezekiel, *Opt. Lett.* **6**, 398 (1981).

³⁴D. F. Walls, *J. Phys.* **6A**, 496 (1973).

³⁵M. D. Levenson and R. M. Shelby, in Proceedings of the Seventh International Conference on Laser Spectroscopy, Maui, 1985 (Springer-Verlag, Berlin, in press).

³⁶J. L. Hall and T. W. Hansch, *Opt. Lett.* **9**, 502 (1984).

³⁷R. M. Gagliardi and S. Karp, *Optical Communications* (Wiley, New York, 1976), Chap. 5.

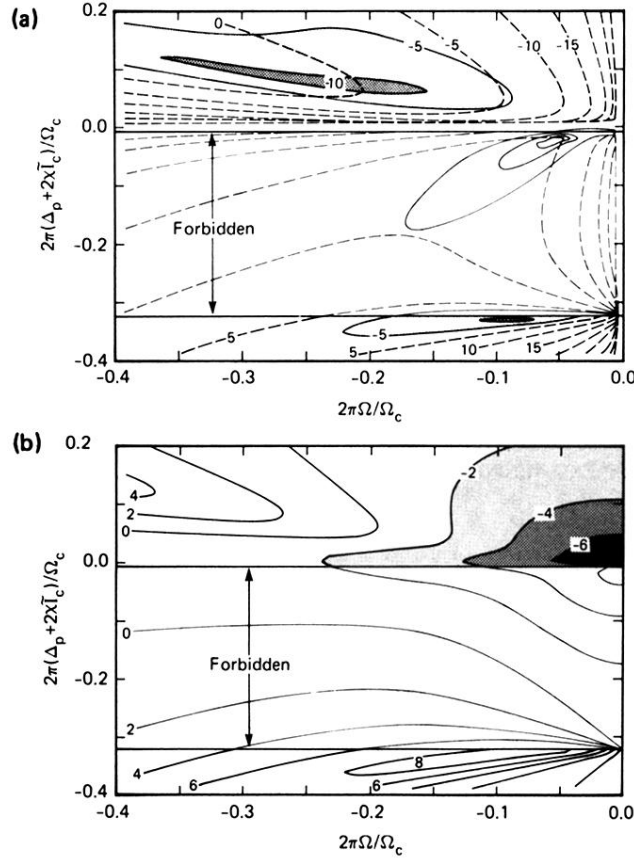


FIG. 5. (a) Contour map of quantum squeezing and GAWBS noise for the bistable case. The phase angle has been chosen to minimize the GAWBS noise as in Eq. (58). The horizontal axis represents the deviation frequency of the noise (as measured on the spectrum analyzer) from $m\Omega_c$. The map has mirror symmetry around $\Omega=0$. The vertical axis represents the frequency shift of the pump laser from the pumped cavity mode as shifted by the optical nonlinearity. Both axes are normalized to the resonator mode spacing $\Omega_c/2\pi$. The dashed lines show the GAWBS noise levels in steps of five decibels from the maximum noise level in a traveling-wave experiment with a similar fiber. These GAWBS contours depend on the value of β . The numbers indicate the noise levels of significant contours. Zero GAWBS noise (i.e., $-\infty$ dB) occurs for $\Omega=0$ and $\Delta_p + 2\chi\tilde{I}_c=0$. The shaded regions are areas where the quantum noise is below the coherent state limit. Again, numbers indicate the suppression in decibels. The forbidden region corresponds to the unstable branch of the bistability state equation. In this figure, the pump detuning is $\Delta_p = -\Omega_c/4\pi$ and the cavity decay rate is $\kappa=0.1$ ($\Omega_c/2\pi$). Quantum squeezing can only be detected when the GAWBS noise is very low. The most promising regions are in the upper left of the figure where significant squeezing is predicted only for $\Omega \approx 0.20$ ($\Omega_c/2\pi$). (b) Contour plot of the sum of the GAWBS and quantum noise at the phase of the minimum of the sum as functions of frequency and pump detuning. The axes are the same as in (a) and the numbers on the contours label the noise level in decibels with respect to the coherent-state limit. In the shaded region the total noise level is below the ordinary quantum limit. For this plot, the GAWBS parameter β was set equal to 5χ . Different ratios of β and χ yield qualitatively similar plots so long as β is less than about 50χ . The best lowest total noise occurs near the point of maximum circulating power and $\Omega=0$. As in (a), $\Delta_p = -\Omega_c/4\pi$ and $\kappa=0.1$ ($\Omega_c/2\pi$).

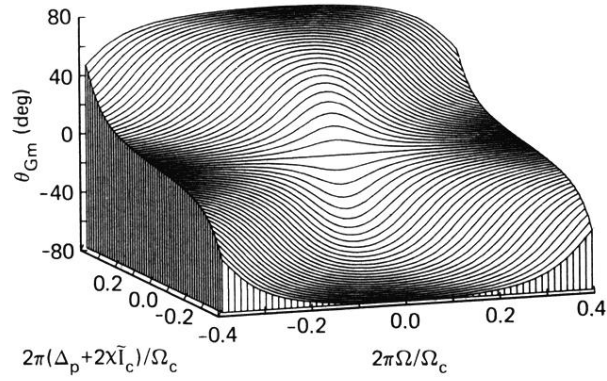


FIG. 9. The phase of the minimum GAWBS noise signal as a function of the detuning of the pump from the resonance of the cavity (as shifted by nonlinear effects) and the detuning of the noise frequency from the cavity-mode spacing. The horizontal axes are normalized to the resonator mode spacing $\Omega_c/2\pi$. When $\Omega=0$ or $\Delta_p + 2\chi\tilde{I}_c=0$, the minimum GAWBS noise is zero. The phase dependence is unaffected by bistability. The cavity decay rate is $\kappa=0.1(\Omega_c/2\pi)$.